Paper 18

From Susceptibility to Magnetization: Advances in the 3D Inversion of Magnetic Data in the Presence of Significant Remanent Magnetization

Li, Y. [1]

1. Center for Gravity, Electrical, and Magnetic Studies (CGEM), Department of Geophysics, Colorado School of Mines, USA

ABSTRACT

Since Exploration '07, tremendous advances have been made in the inversion and quantitative interpretation of magnetic data in the presence of significant remanent magnetization. The advances have occurred on many fronts such as data processing, inversion methodology, as well as practical applications, with contributions from academia, government agencies, exploration and service industries. These advances have significantly extended the utility of 3D magnetic inversions on a wide range of scales in mineral exploration. Theoretically, the single most significant challenge posed by the presence of strong remanent magnetization arises from the unknown direction of the total magnetization, which is the vector sum of the induced and remanent magnetization components. As a direct consequence, the commonly used assumption of equating the magnetization direction to that of the inducing field is no longer valid and renders the inversions based on this assumption invalid. Accordingly, the development of methods to tackle this challenge falls into different categories including various mixed-parameter inversions and generalized inversions, with the latter containing three subcategories: estimating the total magnetization direction for use in inversions, inverting for the magnitude of magnetization from direction-insensitive data derived from total-field anomaly, and directly inverting for magnetization. By far the most diverse development has occurred in the magnetization inversion. A commonality among the diverse approaches is the effort to limit the variability of magnetization and thereby reduce the ambiguity by incorporating geological, petrophysical, or statistical constraints. This paper will review the development and advances along these threads in the last decade, showcase successful applications to illustrate these approaches, and discuss future directions.

INTRODUCTION

Background

Three dimensional magnetic inversion has played an important role in mineral exploration in the last two decades. One of the early results that showcased magnetic susceptibility inversions was presented at Exploration '97 by Watts (1997), who applied the algorithm developed by Li and Oldenburg (1996) and showed the necessity and effectiveness of 3D magnetic inversion in answering a specific geological question of vital importance to the on-going exploration. Since then, many similar algorithms have been developed and improvements have been made (e.g., Pilkington, 1997; Li and Oldenburg, 2000a; Portniaguine and Zhdanov, 2002; Li and Oldenburg, 2003; Fullagar et al., 2008).

Two particular directions of innovation are the algorithms to improve the capability to constrain the solutions through specific model parameterization and incorporation of geological information (e.g., Fullagar and Pears, 2007; Fullagar et al., 2008) and the speed up of large-scale inversion by semi-structured mesh (e.g., Davis and Li, 2013) and by using numerical solution of differential equations governing the magnetic problem (e.g., Lelièvre and Oldenburg, 2006; Davis et al., 2013).

The key assumptions in most magnetic susceptibility inversions are that the magnetization is induced only and that the self-demagnetization effect is negligible, so that the magnetization direction is the same as the inducing field direction. There are two implications from this: (1) the magnetization direction is known; and (2) the susceptibility would be used as the sole physical property to represent the subsurface magnetic sources. In such cases, the magnetic susceptibility is assumed to provide an adequate characterization of the causative bodies. The inversion then focuses on recovering the susceptibility.

There is a large class of exploration problems that can be tackled under these assumptions. However, it is also well recognized that there are more cases with either strong remanent magnetization, or self-demagnetization effect, or both. In such cases, the use of the inducing field direction as the magnetization direction is no longer valid. Consequently, the susceptibility inversion based on weak induced magnetization may not be applicable.

Challenges Beyond Induced Magnetization

The presence of remanent magnetization is common and can occur in rock units having either low or high magnetic susceptibility. The presence of high magnetic susceptibility that leads to self-demagnetization also occurs in some exploration problems. However, it can be argued that the occurrence of remanent magnetization is almost ubiquitous. As the inversion of magnetic data becomes a standard tool to aid interpretation at deposit, district, and regional scales, the need to handle remanent magnetization becomes an important issue.

In "Proceedings of Exploration 17: Sixth Decennial International Conference on Mineral Exploration" edited by V. Tschirhart and M.D. Thomas, 2017, p. 239–260

The total magnetization is the vector sum of an induced component and the remanent component if we assume that both produce fields that are weaker than the inducing field,

$$\vec{J} = \vec{J}_{ind} + \vec{J}_{rem} \quad (1)$$

The direction of the resultant magnetization is unknown if the remanent component is significant relative to the induced component and its direction also differs. The magnetization direction in the presence of high susceptibility can be highly variable due to the geometry dependence of the self-demagnetization effect. The presence of both further compounds the problem and the total magnetization will depend nonlinearly upon the susceptibility and remanent magnetization.

In these cases, the common underlying difficulty is that the direction of the total magnetization is unknown, can deviate significantly from the inducing field direction, and can be spatially variable. Therefore, the inversion ultimately needs to determine both the direction and magnitude of the magnetization distribution.

Mathematically, this is summarized in the following equation,

$$\Delta T(\vec{r}) = \frac{\mu_0}{4\pi} \iiint_V J(\vec{r}')\hat{J}(\vec{r}') \cdot \nabla^T \nabla \frac{1}{|\vec{r} - \vec{r}'|} \cdot \hat{B}_0 \, dv' \quad (2)$$

where both the magnitude, $J(\vec{r})$, and direction, $\hat{J}$, of the magnetization are unknown. In susceptibility inversions, we let $\hat{J} = \hat{B}_0$ when assuming weak induced magnetization. In the presence of significant remanent magnetization $\hat{J}$ is unknown and can be variable. Here, we assume the availability of total-field anomaly data, which constitute the majority of magnetic in exploration. We further assume the total-field anomaly is approximated by the projection of the anomalous magnetic field vector onto the inducing field direction:

The question is then: how can we perform 3D magnetic inversions in such cases, now that we are faced with the task of recovering the magnitude of magnetization in 3D and its direction. This is one of the major areas of advancement in magnetic inversion since Exploration ‘07.

Summary of Major Advances

Many different approaches have been developed to invert magnetic data without knowing magnetization directions. Some are the results of extending and improving those used in the susceptibility inversions while others are innovative new approaches. Not surprisingly, a great many previous developments have become the building blocks for these advances. The variety of methods speaks to the effort and diversity of the potential-field research and development community, and to the importance of the problem. Given the large number of methods published and applied, we focus on those primarily developed for remanent magnetization and group them into the following three categories. They are listed below with subcategories and primary references.

The first category is parametric inversion. This approach seeks to simultaneously invert for both the magnetization and geometrical shapes or boundaries of causative bodies using geometrically simple objects as basic model blocks (e.g., Foss and McKenzie, 2011; Pratt et al., 2012).

The second category is the mixed-parameter inversion using a set of contiguous vertical prisms with movable top and bottom boundaries. This method uses a combined model representation with susceptibility and remanent magnetization and also inverts for the boundaries of geological units (e.g., Fullagar and Pears, 2015).

The third category consists of generalized inversions that seek to invert for a 3D distribution of the magnitude of the magnetization or the magnetization itself (a vector quantity defined by magnitude and direction):

1. Effective susceptibility inversion using estimated total magnetization direction (e.g., Li et al., 2010);
2. Effective susceptibility inversion using converted direction-insensitive data:
    1) Magnetic amplitude data (e.g., Shearer, 2005; Li et al., 2010)
    2) Normalized source strength data (e.g., Pilkington and Beiki, 2013)
3. Magnetization inversion using:
    1) Parameterization in geomagnetic reference frame and specific constraints (e.g., Lelièvre, 2009; Lelièvre and Oldenburg, 2009a)
    2) Compactness model objective function (e.g., Ellis et al., 2012);
    3) Cooperative strategy, amplitude, and magnetic anomalies (e.g., Liu et al., 2013, 2015; Fournier et al., 2016a)
    4) Gramian constraint (e.g., Zhu et al., 2016)
    5) Oriented sparse mixed-norm objective function (e.g., Fournier, 2015; Fournier et al., 2016a);
    6) Fuzzy c-means clustering constraint on magnetization directions (e.g., Li and Sun, 2014, 2016).

As in any discipline, there are certainly numerous efforts that collectively advance the science and practice. In the case of inverting magnetic data affected by remanent magnetization, this is equally true. There is a large amount of works both in the last decade and historically that may not be directly categorized in the framework which this review has settled on, but nonetheless are invaluable.

In the following, we focus the review on the above-listed methods. The levels of details are chosen to enable practicing geophysicists to apply these methods to solve exploration problems. These details are essential to implementing, or to understanding the performance and behavior of the methods. Similarly, we aim to provide as comprehensive as feasible a list of references to benefit both the research and practicing geophysicists.

The focus of this review is on the methods that seek to construct a 3D model of magnetization in the presence of significant remanent magnetization. These methods include and are related to the above-listed inversion methods. The general topic of

remanent magnetization, however, is a much broader field and beyond the scope of this review.

Much pioneering work in remanent magnetization-related interpretation using borehole vector magnetic measurements has been carried out by W. Morris and his collaborators (e.g., Mueller et al., 1997; Morris et al., 2007). Many insights gained in their borehole work are applicable in airborne or ground vector magnetic measurements that are becoming available (e.g., Dransfield et al., 2003). These methods are somewhat beyond the scope of this review paper, so readers are referred to the above-listed and many other publications.

The topic of determining remanent magnetization and total magnetization of isolated bodies is reviewed in an excellent paper by Clark (2014), which includes an extensive list of references. That review paper is highly recommended for anyone researching and using remanent magnetization in applied geophysics.

We will start with the two categories of mixed-parameter inversions for directly recovering magnetization with source geometry. We next proceed to generalized inversions that aim to recover 3D distributions of magnetization (either its magnitude or the magnetization in its vector form). This category has witnessed by far the most variety of advances. We then introduce the exciting direction of geology differentiation based on the inverted magnetization directions. We conclude the review with a brief discussion and look ahead.

PARAMETRIC INVERSION

Historically, parametric inversions in magnetics are perhaps among the oldest magnetization inversions (e.g., Bhattachyryya, 1966) and it is not surprising that renewed research and development associated with remanent magnetization also employed this approach and thrived. Within this context, the traditional least-square parametric inversions have seen the most work.

There have been many developments on this front. Foss and McKenzie (2009, 2011) formulate a parametric inversion that simultaneously recovers the geometrical parameters describing the shapes of a contiguous set of causative bodies and total magnetization vectors that are assumed to be constant within each body. Pratt et al. (2012) fit ellipsoids to estimate the shape and total magnetization of causative bodies. These approaches are extensions of the parametric algorithm used by others (e.g., Silva and Hohmann, 1981; Mueller et al, 1997) to a more flexible parameterization using ellipsoids and dipping prisms with polygonal bases. The solution is obtained through nonlinear least-squares minimization of a data misfit function.

The parametric approach greatly reduces the non-uniqueness that is typically associated with the generalized inversion at the expense of the limited capability for automated inversion of large-scale data sets. However, Foss and McKenzie's (2011) use of many causative bodies each having a possibly different magnetization makes it similar to generalized 3D inversions but having a small number of unknowns. These methods provide a complementary tool set of practical value. Figure 1 illustrates this aspect.

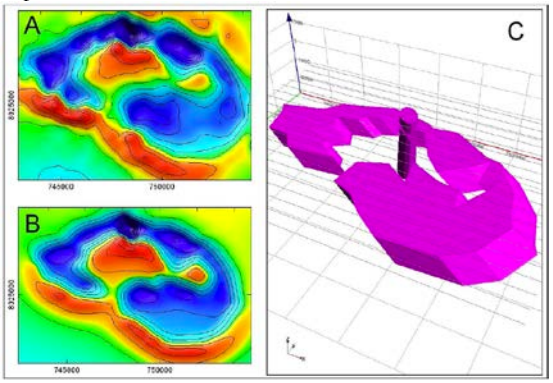

Figure 1: Inversion of total-field magnetic anomaly (a) affected by remanent magnetization by using a group of dipping prisms with polygonal bases and individual total magnetization. (c) (Foss and McKenzie, 2011). Panel (b) shows the predicted data.

COMBINED SUSCEPTIBILITY-MAGNETIZATION INVERSION

Fullagar and Pears (2015) extend their mixed parameterization inversion algorithm using contiguous vertical prisms subdivided into cells with movable top and bottom (e.g., Fullagar et al., 2008). Model cells can belong to different geological units that can carry remanent magnetization in addition to susceptibility. The authors adopt an interesting parameterization consisting of susceptibility and a remanent magnetization vector normalized by the strength of the inducing field to account for both induced and remanent magnetization,

$$\bar{J} = B_0(\kappa' \hat{B}_0 + \bar{q}) \tag{3}$$

where κ' is an effective susceptibility that can account for self-demagnetization and $\bar{q}$ is a normalized remanent magnetization component.

The algorithm can initialize the solution by first recovering a shape for the magnetic body through the inversion of total magnetic gradient (Shearer and Li, 2004) and then sequentially invert for the susceptibility and normalized magnetization vector. In addition "geometry inversion" can be performed (Fullagar et al., 2008) to adjust the 3D shape of the magnetic body. There is also the capability to constrain the magnetic susceptibility to a lower and upper bound estimated for the specific geologic unit. Negative susceptibility is permissible. It is also possible to assign different remanent magnetizations to different geological units. Because of the ambiguity from the mixing of induced and remanent magnetization, the algorithm effectively recovers an optimal vector sum of a component parallel to inducing field direction and a remanent component in an unspecified direction. Depending on the sequence of minimization, the two components can differ but the vector sum remains the same.

Within this framework, the authors have also incorporated self-demagnetization (Fullagar and Pears, 2013) and, thereby,

enabled the full treatment of the magnetic inversion in the presence of both remanent magnetization and high magnetic susceptibility. The latter is a much more challenging problem due to the highly variable resultant magnetization direction.

Figure 2 illustrates the algorithm using a simulated geologic model consisting of an igneous plug intruded into a mixed volcanic and sedimentary terrane. The susceptibility varies within the host rocks but the magnetic properties are assumed uniform in the plug. The igneous plug is highly magnetic and has remanent magnetization that is twice as strong as the induced magnetization. The top panel shows the perspective view of the total-field anomaly and the bottom panel shows a north-south cross-section through the igneous plug. Whether the true susceptibility or zero susceptibility is assigned to the plug, the same resultant magnetization is recovered for the plug over the smoothly varying susceptibility in the host rock. Figure 3 illustrates the companion part of this algorithm in dealing with the self-demagnetization effect, and shows the varying magnetization direction recovered by the algorithm within banded iron formations.

Although the authors did not explore the separation of the induced and remanent magnetization, the algorithm does provide the fascinating opportunity to perform advanced interpretation by examining recovered susceptibility in combination with the magnitude and direction of the remanent magnetization since both are direct results of such an inversion.

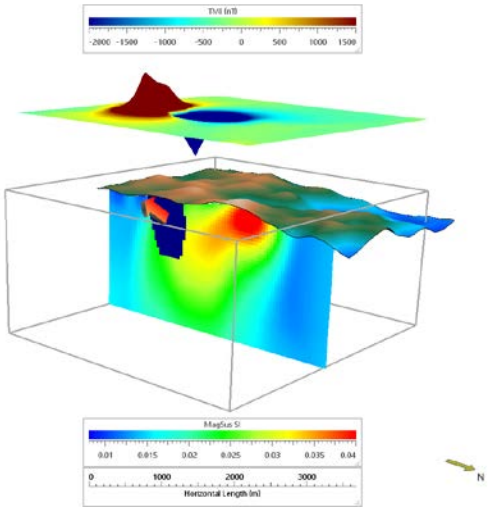

Figure 2: Example illustrating magnetic inversion with remanent magnetization using the vertical prism parameterization. The top panel shows the total-field anomaly. The lower panel shows the recovered causative body with remanent magnetization (direction indicated by the arrow) in a cross-section of background magnetic susceptibility displayed under the topographic surface. (Image courtesy of P. Fullagar and G. Pears).

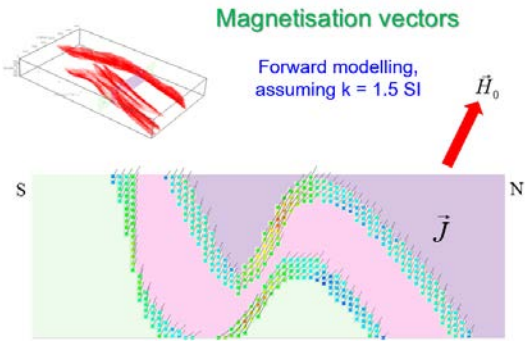

Figure 3: Example illustrating the ability of inversion using VP-parametrization in accommodating a combination of remanent magnetization and self-demagnetization in environments with complex geologic structures. The top-left inset shows the 3D structure of banded iron formation; and the lower panel shows the highly variable total magnetization in a cross-section.

GENERALIZED MAGNETIZATION INVERSION

This category of methods seeks to construct 3D distributions of magnetization ultimately treated as a function of spatial position and represented by a piece-wise constant or similar approximation. This category is characterized by fixed model discretization and inversion for the magnetization. Given this category is a natural extension of the generalized magnetic inversion for 3D susceptibilities in mineral exploration, it is not surprising that many research groups have expended significant effort in developing methods and algorithms to invert for 3D distribution of magnetization.

Since the major challenge in such generalized inversions is the need to simultaneously recover both magnitude and direction of magnetization (i.e., a vector function) and the variability in the direction in a finely discretized model appears to introduce the strongest ambiguity, nearly all algorithms in this category seek to impose some type of constraints to restrict the admissible solutions so that geologically interpretable models of magnetization can be constructed. Furthermore, these constraints either implicitly or explicitly act primarily on the variability of the magnetization direction so the admissible models have limited or coherent magnetization directions.

Magnetization Direction Estimation

As discussed above, the major challenge in quantitative interpretation of magnetic data in the presence of remanent magnetization is the unknown direction of the total magnetization. A natural extension of the susceptibility inversion is to invert for the magnitude $J(\vec{r})$. Thus, a logical sequence is to estimate the magnetization direction first and then invert for the magnitude.

This approach is suitable for interpreting isolated anomalies that are produced by compact source bodies. The estimated direction can then be supplied to equation 2 to invert for the magnitude in the same way as the inversion for susceptibility is carried out. In fact, the existing susceptibility inversion algorithm is directly

applicable if we introduce a concept of effective susceptibility as the ratio of the magnitude of total magnetization over the inducing field strength,

$$\kappa_e = J(\vec{r}) / H_0 = \mu_0 J(\vec{r}) / B_0 \,. \tag{4}$$

The recovered effective susceptibility does not correspond to intrinsic susceptibility, but characterizes the combined magnetization strength due to induced and remanent magnetization components. This is the approach Li et al. (2010) proposed to invert isolated compact magnetic anomalies affected by remanent magnetization. The advantage of this approach is that once a magnetization direction has been estimated, any susceptibility inversion algorithm can solve for the effective susceptibility distribution.

Magnetization direction estimation is a well-studied topic in magnetic exploration and numerous algorithms have also been developed and used in solid earth geophysics. For example, Roest and Pilkington (1993) correlate the total gradient of the magnetic anomaly and the absolute value of the horizontal gradient of the pseudo-gravity produced by 2D sources. This approach inspired Dannemiller and Li (2006) to develop a cross-correlation method in 3D based on the total gradient and vertical derivative of calculated reduced-to-pole (RTP) data. Gerovska et al. (2009) devised a similar method using the amplitude data and the RTP field itself. Fedi et al. (1994) developed a method that minimizes the magnitude of the trough of the calculated RTP field. Lourenco and Morrison (1973) and Phillips (2005) apply the integral relationships of magnetic moments derived by Helbig (1963). Medeiros and Silva (1995) use multipole expansion to estimate the total magnetization direction together with the orientation of the source body. Haney and Li (2002) develop a wavelet-based method for determining magnetization direction from profile data in 2D problems. If gravity or gravity gradient data are also available, then Poisson's relation between the magnetic and gravity gradient tensor can also be used to estimate the magnetization direction, as demonstrated by Cordell and Taylor (1971), Medonca (2004), and Pedersen and Bastani (2016).

Given the importance of the magnetization direction, a large number of publications and algorithms are available for use in practice. Clark (2014) provides a comprehensive review with an extensive reference list.

For this review, we present two methods that are easy to implement, have proved to be effective, and do not require additional information: Helbig's moment method and the cross-correlation methods. The first directly explores the relation between the anomaly and the magnetization direction and computes the magnetization direction from the data, whereas the second estimates the magnetization direction by utilizing the symmetry property of the RTP data. In both methods, the magnetization direction is assumed to be constant within the source.

Helbig's Moment Method

Helbig's method (Lourenco and Morrison, 1973; Phillips, 2005) calculates the components of the magnetic dipole moment, m_x, m_y and m_z, of a compact magnetic source from the first moments of the vector components B_x, B_y and B_z of the anomalous magnetic field. The method is based on the relationships first presented by Helbig (1963), which has the following form in SI units,

$$\begin{aligned} -\frac{2}{\mu_0}\int_{-\infty}^{\infty}\int_{-\infty}^{\infty} xB_z(x,y)dxdy &= m_x \\ -\frac{2}{\mu_0}\int_{-\infty}^{\infty}\int_{-\infty}^{\infty} yB_z(x,y)dxdy &= m_y \\ -\frac{2}{\mu_0}\int_{-\infty}^{\infty}\int_{-\infty}^{\infty} zB_x(x,y)dxdy &= m_z \end{aligned} \tag{5}$$

where μ_0 is the free space permeability, B_x, B_y, and B_z are respectively the three orthogonal components of anomalous magnetic field, m_x, m_y, m_z are respectively the three components of magnetic dipole moment. Assuming that the magnetization direction is constant within the source body, and dipole moment direction determined from the three components by the above equation then provides the magnetization direction.

Two practical issues must be considered in applications. First, we usually have only total-field anomaly data, and need to calculate the three components B_x, B_y and B_z from the total-field anomaly. This can be accomplished using wavenumber domain operators (e.g., Pedersen, 1978; Blakely, 1996; Schmidt and Clark, 1997, 1998) if the observational surface is planar. When the data are located at low magnetic latitudes or on uneven observation surfaces, the equivalent source method of component conversion can be used (e.g., Dampney, 1969; Hansen and Miyazaki, 1984; Li and Oldenburg, 2010).

Second, since Helbig's method is applied over finite data windows while the integrals of B_x, B_y and B_z over the infinite plane of integration are identically zero in theory, care must be exercised to satisfy these conditions within the data window adopted for the calculations.

Cross-Correlation Methods

Dannemiller and Li (2006) developed an estimation method by examining the symmetry of various RTP fields computed for different magnetization directions. Gerovska et al. (2009) developed a similar method using the RTP data and the amplitude of the anomalous magnetic vector. Both methods rely on the fact that the RTP data for a symmetric vertical magnetic body is symmetric. For dipping source bodies such as dykes, the RTP data are the least asymmetric when the correct magnetization direction is used. It follows that the vertical derivative of RTP data is also least asymmetric. The aim is then to find the magnetization direction that minimizes the asymmetry of the computed RTP data.

The asymmetry is gauged by comparing the computed RTP or its vertical derivative with their respective envelope. It has also been shown that the total gradient (amplitude of the gradient vector in 3D) of the RTP anomaly is the envelope of the vertical derivative of the anomaly produced under arbitrary inducing-field and magnetization directions (Nabighian, 1972; Haney et al 2003). The envelope is a function tangential to all members of

the function family, which would be the magnetic anomalies corresponding to different magnetization directions in our case, is the most symmetric form. Since the envelopes cannot be calculated from the total-field anomaly without knowing the magnetization direction, we approximate them by the total gradient, $|\nabla(B_z)|$, and magnetic amplitude data, $\sqrt{B_x^2 + B_y^2 + B_z^2}$, respectively, computed for an assumed magnetization direction.

The symmetry of computed RTP field for an assumed magnetization direction can then be gauged using its cross-correlation with the corresponding amplitude data or using the cross-correlation between the vertical derivative of RTP and total gradient. The adopted inclination and declination estimates are those that maximize the cross-correlation.

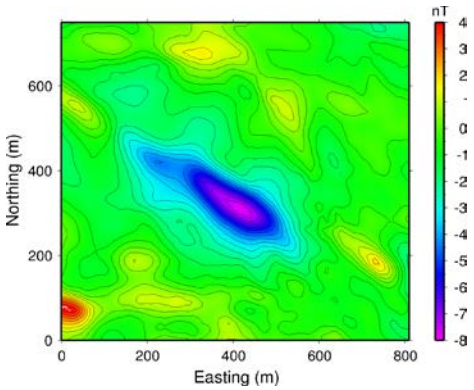

Figure 4: The total-field magnetic anomaly over a kimberlite dyke. The inducing field is in the direction of I=86.7° and D=26.3°. The negative anomaly in the center indicates presence of strong remanent magnetization.

A Field Example

The data set shown in Figure 4 contains a negative anomaly in the center surrounded by several smaller positive ones. The inducing field has an inclination of 86.7º and declination of 26.3º. Given the high magnetic latitude and dominant negative anomaly, it is clear that the kimberlite has strong remanent magnetization and the total magnetization is nearly in the opposite direction to the inducing field. We first estimate the direction for the source of the central negative anomaly and then invert the total-field data to construct the effective susceptibility.

Table 1. Magnetization direction estimated using two different methods for the field data set shown in Figure 4.

Estimation method	Inclination (°)	Declination (°)
Helbig's method	-84.7	70.0
Cross-correlation	-87.4	26.0

The results of estimation are listed in Table 1 for comparison. The estimated values for inclination are similar but the declination varies greatly. This is expected given the inclination is close to -90º. When used in an inversion, the error in declination does not strongly affect the final result either. Using the estimated direction, inversion of total-field anomaly (Figure 4) is shown in one cross-section and one plan section in Figure 5.

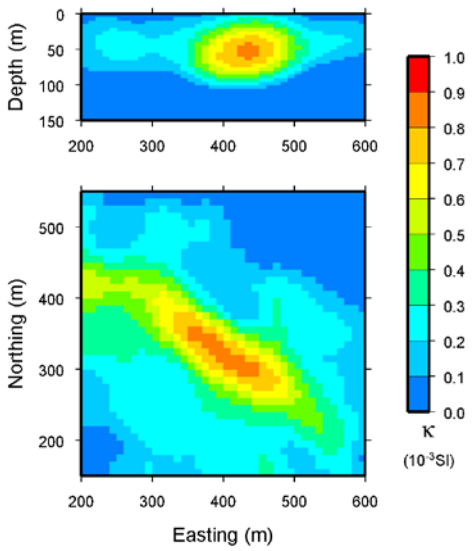

Figure 5: Inverted effective susceptibility obtained by using the estimated magnetization direction from the cross-correlation method. The effective susceptibility is shown in one cross-section at 300-m north (top) and one plan-section at a depth of 50 m (bottom) (Li et al, 2010).

Inversion of Direction-Insensitive Data

The direction estimation approach works well with isolated anomalies, but it is difficult to extend to more complicated cases such as those with multiple overlapping anomalies. In such cases, a reliable direction may not be estimated or the estimate has no real relevance. One logical alternative is to circumvent direction, and use "data" that are derived from the total-field anomaly and have a weak dependence on magnetization direction.

Nabighian (1972) shows that both the total gradient and the magnitude of the anomalous magnetic field vector (henceforth referred to as the amplitude data) are independent of magnetization direction in 2D, and they are envelopes of the horizontal or vertical derivatives of the magnetic anomaly or the total-field anomaly, respectively. Thus, it is feasible in 2D cases to invert for the magnitude of the magnetization without knowing the magnetization direction.

Such direction independent quantities cannot be calculated in 3D cases without knowing the magnetization direction (e.g., Nabighian, 1984; Haney et al., 2003). However, many authors have examined different quantities that are approximately independent of magnetization direction (i.e., weakly dependent upon, or insensitive to, the direction). These include amplitude data and the total gradient (e.g., Nabighian, 1972, 1984; Hou, 1979; Roest et al, 1992; Stavrev and Gerovska, 2000; Haney et al., 2003, Shi et al., 2013), and normalized source strength (NSS) defined by equation 10 (e.g., Wilson, 1985; Beiki et al., 2012). Therefore, one can formulate an inverse problem to

recover the magnitude of the magnetization distribution in the subsurface from one of these transformed data sets without knowing the local magnetization directions (Shearer, 2005; Li et al., 2010; Pilkington and Beiki, 2013).

The forerunners of this approach are Paine et al. (2001), who demonstrated that the vertical integration of the total gradient of the total-field anomaly and the total gradient of the vertical integration of total-field anomaly are both weakly dependent upon magnetization. They treated each of these derived quantities as an approximation to RTP data and inverted them using a susceptibility inversion algorithm. Although treating these quantities as RTP data is not conceptually correct, the underlying idea of using direction-insensitive transformed data is sound.

In contrast to the direction estimation method, the direction-insensitive data approaches have the advantage that they are not limited to a single anomaly nor do they require all anomalies have the same magnetization direction. Therefore, the approach is generally applicable to a wide range of problems in which the source distribution is more complicated.

In the following, we present the basics of algorithm for inverting amplitude data or normalized source strength. The inversion of other direction-insensitive quantities can be carried out in the same manner, as long as one can perform the forward modelling and calculate a descent direction or, better yet, the sensitivity matrix.

Inversion of Amplitude Data

The amplitude data are defined as the length of the anomalous magnetic field vector,

$$B_a = \left|\mathbf{B}_a\right| = \sqrt{B_{ax}^2 + B_{ay}^2 + B_{az}^2} \tag{6}$$

where B_a is the amplitude and (B_{ax}, B_{ay}, B_{az}) are the three orthogonal components of the magnetic anomaly vector. Although amplitude data do have some dependency on magnetization direction in 3D, the dependency is rather weak.

Figure 6 illustrates this weak direction dependence. The causative body is made up of two horizontal segments of vertical dykes with different strike directions and variable depth to the top. The inducing field has an inclination of -5º and a declination of 0º. The column on the left shows the total-field anomaly for two different magnetization directions, one aligned with the inducing field and another nearly perpendicular. The second case simulates the presence of strong remanent magnetization. The column on the right shows the corresponding amplitude data. While the total-field anomalies in the two cases are markedly different, the amplitude data are much more similar and provide a good indication of the horizontal location of the causative body.

This direction-insensitivity of amplitude data is advantageous for interpretation of magnetic data in the presence of remanent magnetization. The amplitude data can be inverted to recover a 3D distribution of magnitude of the magnetization (Shearer, 2005; Li et al, 2010), represented by the effective susceptibility.

To invert amplitude data, we must first calculate the amplitude data from the observed total-field anomaly data. The three magnetic anomaly components may be converted from the total-field anomaly using wavenumber-domain expressions (e.g., Pedersen, 1978) when the data are located on a plane or equivalent source techniques (Dampney, 1969) if the data lie on uneven observational surfaces or located at low magnetic latitudes.

The formulation of amplitude inversion assumes the availability of three-component data for calculating the amplitude data but places no restrictions on the strength of the anomalous field. The above-mentioned approaches for calculating amplitude data via conversion of total-field anomaly to three-component anomaly, however, assume that the anomalous field is much weaker than the inducing field and the total-field anomaly is well approximated by the projection of the anomalous field vector onto the inducing field direction. This assumption may be a limit in practical applications in highly magnetic environments. However, the availability of directly measured three-component magnetic data would remove this limitation.

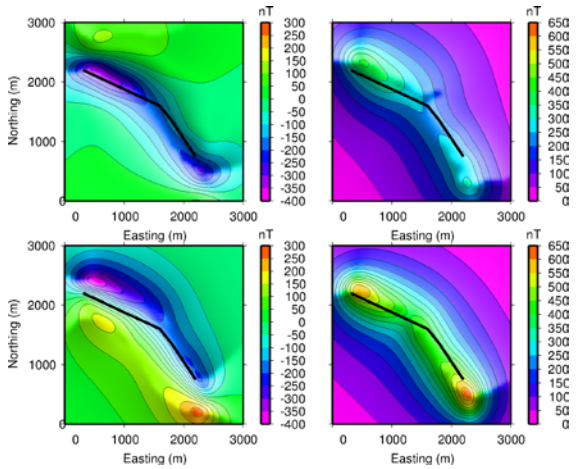

Figure 6: Comparison of amplitude data for two different magnetization directions. The top row displays the total-field anomaly and amplitude data at low latitude (I=-5º) produced by induced magnetization. The black lines indicate the projection of the source location on the surface. The bottom row shows the corresponding quantities when the magnetization is nearly vertical under the same inducing field. The total-field anomalies are drastically different, yet the corresponding amplitude data are much more similar.

For computational purposes, we can adopt a model representation that discretizes the 3D model region into a set of contiguous rectangular cells, and assume a constant effective susceptibility value within each cell. In such a model, each component of the magnetic anomaly vector is given by a matrix-vector product in the same way as for total-field anomaly,

$$\vec{d}_x = \mathbf{G}_x\vec{\kappa}, \quad \vec{d}_y = \mathbf{G}_y\vec{\kappa}, \quad \vec{d}_z = \mathbf{G}_z\vec{\kappa}, \tag{7}$$

where $\vec{d}_x = (B_{x1}, \cdots, B_{xN})^T$ is a vector containing the x-components of the anomalous magnetic field, $\vec{d}_y$ and $\vec{d}_z$ contain the corresponding y- and z-components, $\vec{\kappa} = (\kappa_{e,1}, \cdots, \kappa_{e,M})^T$ is the vector of unknown effective susceptibilities to be recovered, and $\mathbf{G}_x$, $\mathbf{G}_y$, and $\mathbf{G}_z$ are the sensitivity matrices relating the anomalous magnetic field components to the effective susceptibilities.

Combining equations 6 and 7 yields the requisite forward mapping that relates the amplitude data to the effective susceptibility model. This relationship is nonlinear and we have a nonlinear inverse problem.

To perform the inversion, a standard Tikhonov regularization approach similar to that used for conventional susceptibility inversion can be used. This is the approach used by Shearer (2005) and Li et al (2010). The solution is obtained iteratively.

An important component of amplitude inversion is the calculation of the Jacobian matrix, whose elements are the partial derivative of the amplitude data with respect to the effective susceptibility. A closed form solution based on the inner production of the magnetic anomaly vectors of the entire model and a given model cell, respectively, is presented by Li et al (2010).

Coleman and Li (2012) and Coleman (2014) examine the error propagation from total-field anomaly to the calculated amplitude data. To a first order approximation, the standard deviation of the computed amplitude data is the same as that of the total-field anomaly. This relationship enables us to define a target amplitude data misfit and choose the optimal regularization during the inversion of amplitude data that are computed from total-field anomaly.

The inversion of amplitude data has been applied successfully to a wide range of data sets in exploration settings. Li et al. (2012) apply the method to image volcanic units in a basin environment for gas exploration; Li and Li (2014) apply the method to image an intrusive complex whose contact with limestones forms the favorable zone of magnetite deposit; Leao-Santos et al. (2015) use it to characterize an iron oxide copper gold (IOCG) deposit near the magnetic equator.

A Field Example

Figure 7 shows the total-field anomaly and the corresponding amplitude data computed through an equivalent source method at the Furnas South deposit located in the Carajás Mineral Province, in the northern region of Brazil (Leao-Santos et al. 2015). The magnetic anomaly is produced by a tabular magnetite-rich orebody. The ambient field has an inclination of −5.7° and a declination of −19.8°. It is clear that these anomalies do not have the pattern that would be produced by induced magnetization at this low magnetic latitude. The unusual pattern was cause by the combination of three factors including the presence of strong remanent magnetization, self-demagnetization, and an anisotropic magnetic susceptibility. The end result is a magnetization closer to vertical than to the inducing field. The peak of calculated amplitude exhibits an excellent correspondence with the horizontal location of the orebody.

The inversion of the amplitude data produced a 3D effective susceptibility distribution that is consistent with known geology and images orebodies delineated by extensive drill holes, as shown in a cross-section in Figure 8 and in 3D in Figure 9.

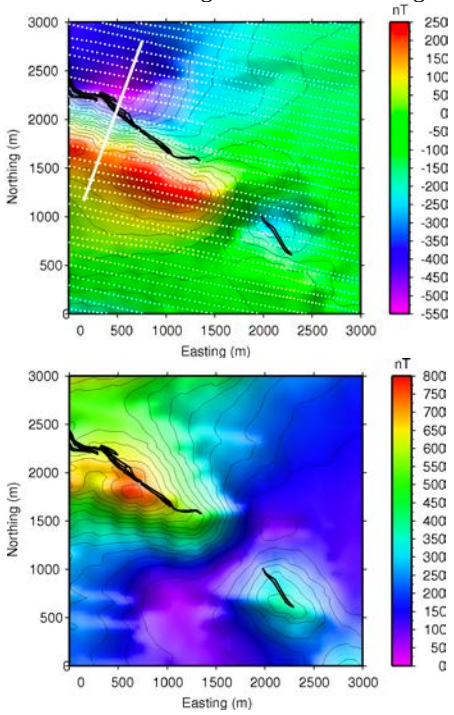

Figure 7: The total-field magnetic anomaly from an airborne survey (top). The local inducing field is in the direction of I = −5.7º and D = −19.8º. Magnetic amplitude calculated from the total-field anomaly (bottom). The black lines indicate the horizontal location of high-grade ore and the white line indicates the position of a geologic section for comparison (after Leao-Santos et al, 2015).

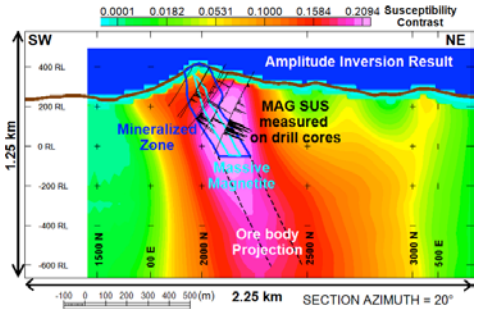

Figure 8: The comparison between the inverted effective susceptibility from amplitude data and the known geology in a cross-section indicated in Figure 7. The recovered effective susceptibility model (color contour) has characterized the massive magnetite (outlined in light blue), and the known mineralized zone in dark blue. Measured magnetic susceptibilities are also shown along several drill holes (after Leao-Santos et al, 2015).

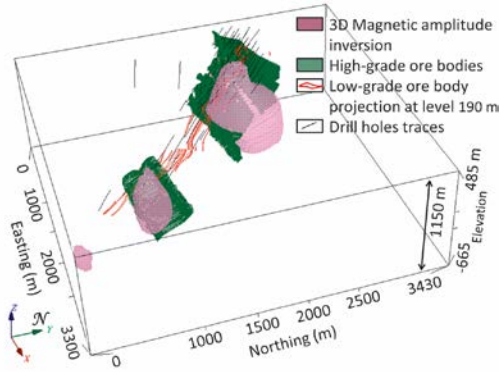

Figure 9: 3D comparison of the recovered effective susceptibility model (pink) with the known ore bodies (green) in the 3D geological model of the high-grade mineralization zones constructed from extensive drilling in the Vale-Furnas Project (after Leao-Santos et al, 2015). The overlapping volume (purple) indicates the consistency between the two models.

Inversion of Normalized Source Strength

Another interesting development in this subcategory is the inversion of NSS derived from the magnetic gradient tensor by Pilkington and Beiki (2013). The use of NSS dates back to 1980s in a host of publications on magnetic target identification by examining the eigenvalue decomposition of magnetic gradient tensor, $\mathbf{T} = \nabla \vec{B}_a^T$, produced by a dipole source at an observation location. The tensor admits an eigenvalue decomposition,

$$\mathbf{T} = \mathbf{R}\boldsymbol{\Lambda}\mathbf{R}^T, \tag{9}$$

where $\mathbf{R}$ is an orthonormal eigenvector matrix and $\boldsymbol{\Lambda}$ is the eigenvalue matrix with the eigenvalues in descending order $\lambda_1 > \lambda_2 > \lambda_3$ as diagonal elements. Wilson (1985) defines a tensor invariant quantity,

$$\mu = \sqrt{-\lambda_2^2 - \lambda_1\lambda_3}, \tag{10}$$

which is proportional to the dipole moment but independent of its orientation. This invariant, termed the NSS, is also inversely proportional to the fourth power of the distance from the sensor to the source. Thus,

$$\mu = \frac{\mu_0}{4\pi}\frac{3|\vec{m}|}{|\vec{r} - \vec{r}_s|^4}. \tag{11}$$

Where $|\vec{m}|$ is the dipole moment, $\vec{r}_s$ and $\vec{r}$ are respectively the source location and observation locations.

The direction-independent property of the NSS holds strictly true only in the case of a dipole or spherical source (e.g., Schmidt et al., 2004) and does not extend to arbitrary 3D sources. Nonetheless the NSS is weakly dependent on the direction in general and has been employed for 3D interpretation of magnetic data (e.g., Beiki et al., 2012; Clark, 2013).

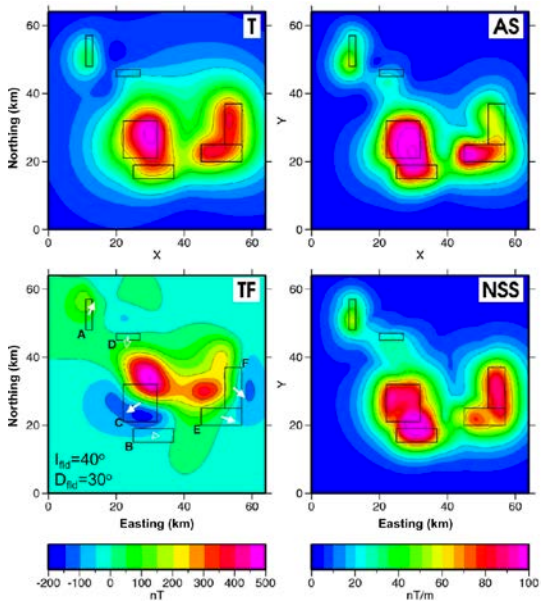

Figure 10: Comparison of calculated NSS with the amplitude data (T), total gradient (AS), and total-field anomaly (TF) produced by a set of prisms with differing magnetization directions (Pilkington and Beiki, 2013).

Figure 10 is reproduced from Pilkington and Beiki (2013) to illustrate the weak dependence of NSS upon magnetization direction. It compares the total-field anomaly produced by six prisms having different magnetization directions with transformed amplitude data, total gradient, and NSS. The total-field anomaly is complicated, whereas the NSS, amplitude, and total gradient peaks coincide quite closely with the magnetic bodies.

To perform NSS inversion, one must first convert the total-field anomaly to three orthogonal components (B_{ax}, B_{ay}, B_{az}) and further compute their derivatives to generate the gradient tensor. Applying an eigenvalue decomposition to the computed gradient tensor at each location then yields the eigenvalues required for NSS. The calculation of gradient tensor adds a level of complexity and care must be taken to avoid the amplification of noise in the derivative calculations. If the gradient tensor is measured, then it can be used directly in the decomposition. Pilkington and Beiki (2013) use the Tikhonov regularization formalism to invert NSS, and carry out the minimization of the total objective function using a gradient descent method.

As a field example, Figure 11 shows part of a data set from the Jean Marie River area, Northwest Territories, Canada (Pilkington and Beiki, 2013). The different patterns of the two total-field anomalies indicate the presence of strong remanent magnetization. The calculated NSS shows two compact anomalies. The inversion of these NSS data produces two similar magnetic bodies with spatial configurations (Figure 12).

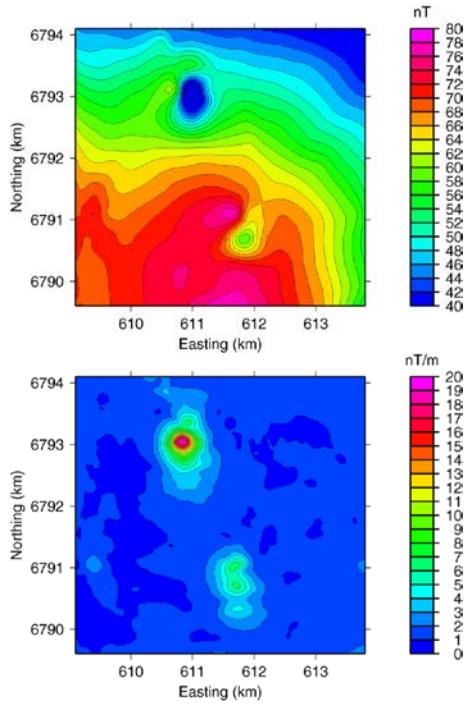

Figure 11: Top panel shows total-field anomalies from Northwest Territories, Canada. The inducing field has I=79^o and D=21^o. The lower panel shows the calculated NSS (Pilkington and Beiki, 2013; image courtesy of M. Pilkington).

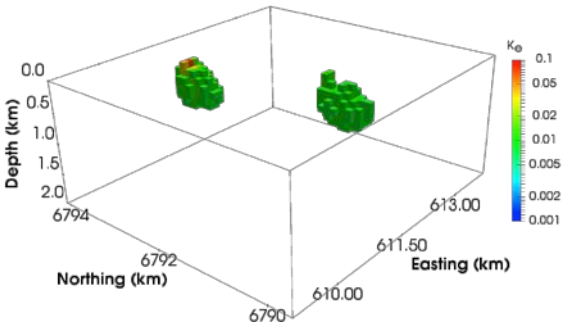

Figure 12: 3D effective magnetic susceptibility model recovered by inverting the calculated NSS in Figure 11. A cutoff value of 0.01 SI is used to display the high-susceptibility regions of the model. (after Pilkington and Beiki, 2013).

Magnetization Inversion

The primary difficulty with the inversion of magnetic data affected by remanent magnetization is the unknown magnetization direction. The approaches discussed in the two preceding subsections seek either to estimate the direction prior to inversion or to circumvent the need for the direction in the inversion. In both cases inversion produces a 3D model of magnetization magnitude. Ideally, we would like to recover the magnetization vector fully, both its magnitude and direction.

The corresponding inverse problem is highly non-unique since a vector magnetization inversion seeks to recover three functions in a 3D space. The magnetization can be represented by its three components or by its magnitude and direction, i.e. inclination and declination. However, we only have a 2D magnetic data set. Therefore the associated ambiguity is much more severe than that encountered in the inversion for one scalar function such as magnetic susceptibility or the magnitude of magnetization. Thus additional conditions are required to select magnetization distributions with the characteristics preferred by the user. These additional conditions on the magnetization or direction are typically imposed through explicit constraints or by augmenting the objective function. There have been a large number of published works on magnetization inversion. Although it remains an active area of research, many algorithms are now available for application in exploration.

Wang et al. (2004) present an algorithm for determining the total magnetization direction of separated, homogeneous bodies. Kubota and Uchiyama (2005) present least-squares inversion for 3D distributions of magnetization in seamount studies. Lelièvre and Oldenburg (2009a) present a comprehensive study of magnetization inversion, in which the authors discuss two alternative parameterizations and explore the need to impose geological constraints to produced interpretable magnetization models. Ellis et al. (2012) present a similar algorithm and employ an objective function which imposes compactness on the magnitude of magnetization. Liu et al. (2013) developed a magnetization inversion for borehole data by starting from the inversion of amplitude data. Zhu et al. (2015) developed a Gramian-constrained magnetization inversion. Fournier (2015) and Fournier et al. (2016a and 2016b) developed an oriented sparse mixed-norm objective function to constrain both the spatial distribution and direction variation of magnetization. Li and Sun (2014, 2016) developed a magnetization inversion by statistically constraining the variations of magnetization direction using fuzzy c-means (FCM) clustering. These algorithms have similar essential parts and differ primarily in what the constraints are imposed on magnetization direction. We note that the combined susceptibility-magnetization inversion discussed in "Combined Susceptibility-Magnetization Inversion" is also a form of magnetization inversion that yields 3D total magnetization vector models.

Working with magnetization direction can be challenging but the reward lies in the potential to extract additional information from the magnetization directions since the remanent magnetization carries information about the formation and geological history of the magnetic units. Therefore, any advancement in magnetization inversion will not only help overcome the numerical difficulties arising from the unknown magnetization direction, but also provide an opportunity for magnetic source characterization and geological differentiation.

In this section, we discuss briefly six magnetization inversion algorithms that employ different parameterization and inversion approaches. We assume total-field magnetic anomaly $\vec{d}^{obs} = (\Delta T_1^{obs}, \cdots, \Delta T_i^{obs}, \cdots)^T$ produced by a 3D distribution of magnetization $\vec{J}(x, y, z)$ and we represent the 3D function of magnetization by a set of contiguous rectangular cells.

Assume that each cell has a uniform magnetization $\vec{J}_j = (J_{xj}, J_{yj}, J_{zj})$. For convenience, we represent the magnetization by its three Cartesian components, and define the model for the inverse problem as the algebraic vector formed by concatenating the three components of the total magnetization vectors,

$$\vec{m} = \begin{pmatrix} \vec{J}_x \\ \vec{J}_y \\ \vec{J}_z \end{pmatrix}, \tag{12}$$

where $\vec{J}_x$, $\vec{J}_y$, and $\vec{J}_z$ contain the three components of the total magnetization in model cells. The forward modelling is then given by the following equation,

$$[G_x, G_y, G_z]\vec{m} = \vec{d} \tag{14}$$

where G_x, G_y, and G_z are respectively the sensitivity matrices of the total-field anomaly with respect to the x-, y-, and z-components of total magnetization.

Magnetization inversion is usually formulated in terms of Tikhonov regularization and the vector magnetization distribution is found by minimizing the objective function,

$$\phi(\vec{m}) = \phi_d(\vec{m}) + \beta\phi_m(\vec{m}), \tag{15}$$

where $\phi_d(\vec{m})$ is the data misfit function and $\phi_m(\vec{m})$ the model objective function.

For different implementations that impose special constraints, authors have also used similar representation but in rotated coordinate systems that are either local or global within the model domain (e.g., Lelièvre and Oldenburg, 2009; Fournier et al., 2016). We will review these in specific section below.

Magnetization Inversion in Inducing-Field Reference

Lelièvre (2009) and Lelièvre and Oldenburg (2009a) developed a full 3D magnetization inversion algorithm employing two different parameterizations. They design these parametrizations explicitly for imposing constraints for dealing with the increased ambiguity in the inversion for magnetization.

In the first approach, magnetization is represented in a Cartesian reference frame aligned with the inducing field direction. The primary direction is the inducing field, $\hat{p} = \hat{B}_0$, and additional two directions $\hat{S}$ and $\hat{q}$ perpendicular to $\hat{B}_0$ completes the orthogonal trio (Figure 13). The magnetization in each cell is then defined by the three components in this coordinate system,

$$\vec{J}_i = p_i\hat{p} + s_i\hat{s} + q_i\hat{q}. \tag{16}$$

This reference frame can be considered as a rotated version of that used in equations 12 and 13 because the three directions remain constant throughout the model domain. This is referred to as TMVC, where C stands for Cartesian.

In the second approach, the authors explicitly represent the magnetization by its magnitude, inclination, and declination. The parameterization is in a spherical coordinate system and related to the Cartesian components by the standard geomagnetic projection in the right-hand Cartesian system with x-axis pointing north (e.g., Blakely, 1996). The authors refer to this parametrization as TMVS, where S stands for spherical. The advantage of TMVS is that it is more convenient to imposing direction-based constraints on the magnetization direction.

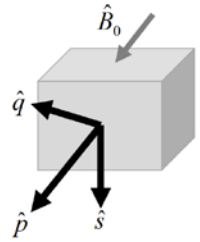

Figure 13: The parameterization of magnetization in the inducing-field reference frame. $\hat{p} = \hat{B}_0$ is the inducing field direction and $\hat{S}$ and $\hat{q}$ are two perpendicular directions.

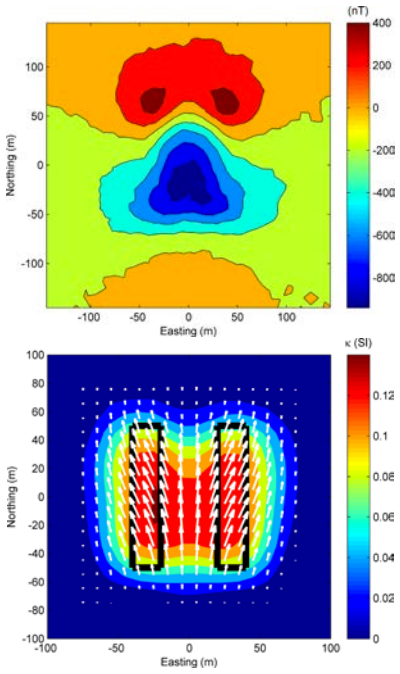

Figure 14: A synthetic example with two source bodies having differing magnetization directions. Top panel shows the total-field anomaly. Bottom panel is a plan section through the recovered 3D magnetization model. The color contour shows the recovered effective susceptibility, arrows the inverted magnetization direction. The black rectangles outline the position of the source bodies. (Lelièvre and Oldenburg, 2009a).

The interesting aspect of TMVC, however, is that it partitions the total magnetization into one part that is parallel with the inducing field and second part $s_i\hat{s} + q_i\hat{q}$ that must be purely remanent. This partition essentially allows one to control the amount of remanent magnetization orthogonal to the inducing field during the inversion. To facilitate this, Lelièvre and Oldenburg (2009a) use the following model objective function,

$$\phi_m = \left\|\mathbf{W}_p\vec{p}\right\|^2 + \rho\left\|\mathbf{W}_s\vec{s}\right\|^2 + \rho\left\|\mathbf{W}_q\vec{q}\right\|^2, \qquad (17)$$

where ρ is an adjustable parameter, and $\mathbf{W}_p$, $\mathbf{W}_s$, and $\mathbf{W}_q$ are model weighting matrices corresponding to commonly used model objective functions consisting of a smallness term and three flatness terms. When $\rho \to 0$, there is no restriction on the size of the s- and q- components; while when $\rho \to \infty$ the magnetization is aligned with the inducing field direction. The component parallel to the ambient field is often predominantly induced. The choice of ρ value is dictated by the available prior information, so this parameter becomes a versatile vehicle for imposing different constraints.

Lelièvre and Oldenburg (2009a) discuss in detail how to impose various types of prior information such as known total magnetization direction, measured magnetic susceptibility, measured Königsberger ratio (Q), or estimated remanent magnetization direction.

An example of magnetization vector inversion is shown in Figure 14 (after Lelièvre and Oldenburg, 2009a). The model consists of two parallel rectangular bodies with NW and NE magnetization directions. Because of the proximity of the two sources, their total-field anomalies merge (Figure 14a – top). The total magnetization inversion is able to recover the source region of high magnetization strength (Figure 14 - bottom). The magnitude of the magnetization exhibits a smooth variation whereas the recovered magnetization directions are distinctly different in the west and east part of the model. This example also illustrates the importance and potential utility of magnetization direction recovered from the inversion. Although the recovered magnetization strengthen does not indicate the presence of two separate causative bodies in this example, the magnetization directions clearly shows that two different source regions are present.

Figure 15 shows the result Lelièvre and Oldenburg (2009a) obtained from inverting a set of field data acquired in southern hemisphere. The total-field anomaly map shows two distinct negative anomalies without visible positive lobes, which indicates clearly the presence of strong remanent magnetization. Their magnetization inversion was necessary to invert this data set and recover the two separate source bodies. Although not reproduced here, the magnetization in one part of the model deviates significantly from the inducing field direction in contrast to the rest of model. The difference suggests that part of the magnetic body is distinctly different.

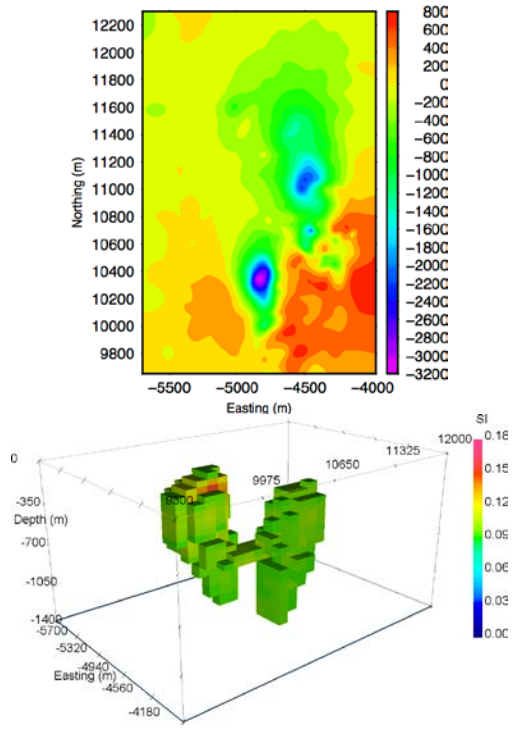

Figure 15: Field example of magnetization inversion using the parametrization in the inducing-field reference frame (Lelièvre and Oldenburg, 2009). Top panel shows the total-field anomaly with two negative anomalies. The inducing field direction at the site is I=-32.2º and D=-0.8º. The lower panel shows the magnitude of recovered magnetization. (Image courtesy of P. Lelièvre).

Compact Magnetization Inversion

Ellis et al. (2012) developed a similar approach to invert total-field magnetic data to recover a 3D distribution of total magnetization vector. They employed a Tikhonov regularization formulation and used a standard data misfit function as well as a model objective function emphasizing compactness of the magnetization vector model. Although the details of the algorithm are not available in published literature, the numerical results in synthetic and field examples show coherent magnetization directions. MacLeod and Ellis (2013) further illustrate the algorithm by applying it to different data sets and compare the result with unconstrained susceptibility inversion.

Figure 16 from MacLeod and Ellis (2013) compares the result using magnetic vector inversion algorithm with an unconstrained susceptibility inversion that allows the susceptibility to be either negative or positive. The negative values would be equivalent to a reversed magnetization which could have arisen during a magnetic field reversal.

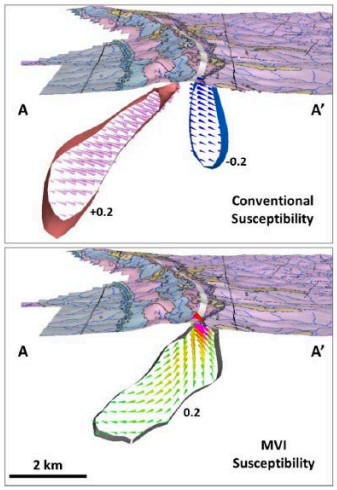

Figure 16: North-south cross-section through the unconstrained susceptibility model (top) and magnetization model (bottom) produced by MacLeod and Ellis (2013), displayed below the topographic surface with geology overlay. The magnetization vector is shown as cones in both cases together with the isosurfaces of effective susceptibility. The warm color indicates higher magnetization magnitude. (Image from MacLeod and Ellis, 2013).

The unconstrained susceptibility inversion produces two zones with significant susceptibility, one with negative values and the other with positive values. Such a model is inconsistent with the single causative body associated with the ore body expected from known geology. Using the algorithm that favors compactness of magnetization anomaly, the inversion is able to produce a single dipping causative body, which is more interpretable geologically. The corresponding magnetization directions vary coherently within the body and a portion of them significantly different from the ambient magnetic field direction. In this case the inversion appears to have produced an improvement over conventional susceptibility inversion.

Cooperative and Sequential Inversion for Magnetization

As discussed earlier, the amplitude data are strictly independent of magnetization direction in 2D (Nabighian, 1972). Liu et al. (2013) leverage this property and apply amplitude inversion (Shearer, 2005; Li et al., 2010) to vector borehole data with a 2D-source assumption. The authors compute the amplitude data from vector magnetic data recorded in the boreholes. An interesting and practically important aspect of their work is the fact that the amplitude data are computed from directly measured components.

Liu et al. (2013) discretize the 2D section between boreholes into a set of contiguous rectangular cells and assume a constant magnetization magnitude for each cell. They seek to recover magnetization magnitude models with a data misfit below a user-specified threshold to image the spatial extent of the causative bodies. Given a magnetization magnitude model, the observed vector magnetic data are inverted in a second step to predict magnetization direction.

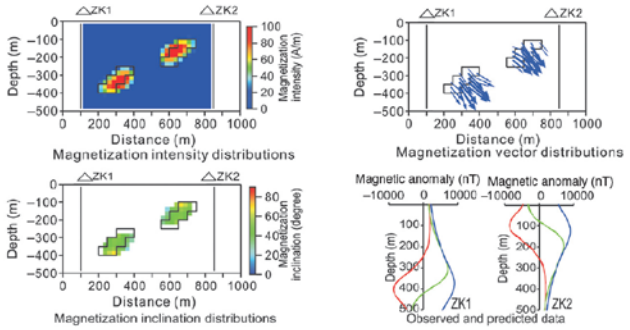

Figure 17: A synthetic illustration of 2D magnetization inversion using amplitude data (blue profiles in low-right panel) derived from borehole vector magnetic measurements. The top-left panel shows the magnetization magnitude recovered from amplitude data; the lower-left and top-right panel show the inclination and projection of magnetization vectors recovered from fitting the vector magnetic data. (Image from Liu et al. 2013).

Figure 17 is a synthetic illustration of the method by Liu et al. (2013) using two causative bodies located between two vertical boreholes. As a technical demonstration, Figure 18 shows application of the method to amplitude and vector magnetic data in three boreholes intersecting a dipping massive magnetite body.

Liu et al. (2015) extend this approach to surface 2D data by first inverting the amplitude data for the magnetization magnitude and then use a cross-correlation between observed and predicted total-field anomaly to estimate the magnetization direction. The assumption is that multiple causative bodies have the same magnetization direction.

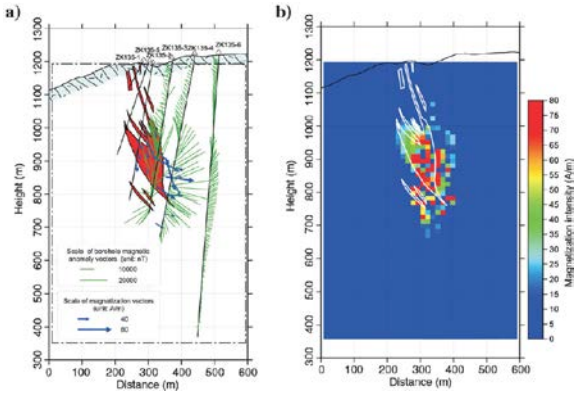

Figure 18: Field 2D data example from Liu et al. (2013) showing (a) the magnetization direction after second stage fitting of vector magnetic data and (b) recovered magnetization magnitude model after inversion of borehole amplitude data. (Image from Liu et al 2013).

Gramian-Constrained Inversion

Zhu et al. (2015) develop a Gramian-constrained magnetization inversion algorithm. The algorithm essentially requires that a

component of the magnetization is linearly correlated with the magnitude of the magnetization through the minimization of a quantity termed Gramian as a part of the objective function. The Gramian is a measure of similarity between vectors. For the vectors $\vec{\kappa}_e$ and $\vec{\kappa}_x$, the Gramian, S_{Gx}, is defined by an inner product matrix,

$$S_{Gx} = \begin{vmatrix} \langle \vec{\kappa}_e, \vec{\kappa}_e \rangle & \langle \vec{\kappa}_e, \vec{\kappa}_x \rangle \\ \langle \vec{\kappa}_e, \vec{\kappa}_x \rangle & \langle \vec{\kappa}_x, \vec{\kappa}_x \rangle \end{vmatrix}, \quad (18)$$

where $\vec{\kappa}_e$ and $\vec{\kappa}_x$ could for example contain respectively the magnitude and *x*-component of the magnetization in the model. To better understand the Gramian, note that it can be expressed as,

$$S_{Gx} = |\vec{\kappa}_e|^2 |\vec{\kappa}_x|^2 \sin^2\theta \quad (19)$$

where θ is the angle between the two algebraic vectors. Therefore to minimize the Gramian between two model vectors is to optimize the angle between the two model vectors so they are either maximally aligned or anti-parallel.

Zhu et al. (2015) include Gramians associated with the three magnetization components in their objective function and minimize them in a Tikhonov regularization formulation (equation 15). The minimization of Gramians acts to enhance coherency of magnetization directions of model cells. Magnetization inversion with Gramian constraints may be applicable for inversion of a single anomaly or of multiple anomalies with same total magnetization direction.

Figure 19 shows the comparison between the true and recovered magnetization model from a minimum Gramian inversion. Three components of the models are shown in one cross-section. The Gramian constraint has produced a magnetization distribution that is quite consistent with the dipping slab in the true model despite the lack of any constraints on the shape of the source body.

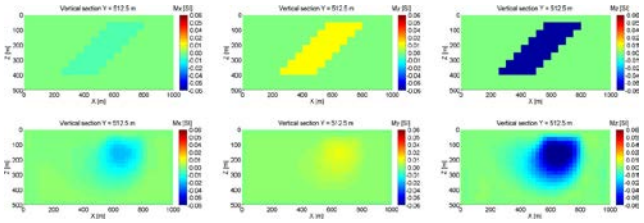

Figure 19: Synthetic example illustrating the Gramian-constrained magnetization inversion. The top row shows the three components (in effective susceptibility) of a 3D dipping slab. The bottom row shows the corresponding components in the inverted model. (After Zhu et al., 2015).

Oriented Mixed-Norm Inversion

In their extensive research on magnetization inversions, Fournier (2015) and Fournier et al (2016a, 2016b) have focussed on sparse mixed-norm objective functions. The strategy is complementary to many efforts in the last decade in that the authors identify necessary parameters for data-set adaptive model objective functions to refine the structural definition of the recovered magnetization model, which in turn restricts the admissible variations of magnetization directions.

The model objective functions are designed to control two model characteristics, namely, the strike and dip of the causative bodies (orientation) and the smallness and flatness of the recovered model (sparseness). The orientation defined by the strike and dip of subsurface anomalous bodies are adaptively applied to different regions of the model domain through local rotations of the coordinate system for calculating the derivatives in the flatness terms, while the sparseness is controlled by applying different *Lp* norms to the smallness and flatness components.

The model objective function is given by,

$$\phi_m = \alpha_s \iiint |\, m - m_{ref}\,|^p \, dv + \sum_{i=1}^{3} \alpha_i \iiint \left| \frac{\partial m}{\partial x_i} \right|^q dv, \quad (20)$$

where m is the model, which could either be the magnitude of the magnetization or the magnetization vector, and m_{ref} the corresponding reference model. The exponents p and q are applied in the norms for the smallness and flatness terms, respectively, and they are chosen to be different to incorporate specific prior information. The variables x_1, x_2, and x_3 are the rotated local coordinate axes at each location in the 3D model and they are different from the fixed user coordinate system (e.g., Li and Oldenburg, 2000b; Lelièvre and Oldenburg, 2009b).

The rotated local coordinates are aligned with the structural orientations of the model features to be recovered. The flatness or blockiness can be imposed adaptively at different locations within the model based on the information about the model structures and their orientations, which can be available a priori or estimated from the magnetic data. Fournier et al (2016a, 2016b) devise an elaborate scheme to compute the partial derivatives using a finite difference stencil involving 26 forward and backward finite differences. The parameters q and p indicate different norms for the smallest model and the flatness terms.

Fournier et al (2016a, 2016b) also explicitly choose to use different values for exponents p and q to take advantage of compact L_0 and blocky Lp norm ($1 < p < 2$) in equation 20 (e.g., Sun and Li, 2014). The flatness terms in the rotated local coordinates enable the construction of models with blocky and smooth features in arbitrary orientations through the L_2 norms, while the compact L_0 norm in the smallness term favors construction of sparse models. Thus, a common choice of the authors is p=0 and q=2.

The sparsity and coherency of recovered magnetization anomalies in the model domain then implicitly place a strong constraint on the variability of the magnetization direction, which enables the recovery of magnetization models with coherent directions from inverting total-field magnetic anomalies.

To implement the mixed-norm objective function, the authors employ the Ekblom norm (Ekblom, 1973) and its numerical solution by the iteratively reweighted least-square approach (IRLS), which the authors further improve by introducing a scaling term in the reweighting factor. The approach is termed the scaled-IRLS (S-IRLS) (Fournier, 2015; Fournier et al., 2016a, 2016b).

Using such a highly adaptive model objective function and the improved numerical solution strategy S-IRLS, the authors develop a cooperative magnetization inversion. The starting point is the magnetization magnitude recovered by inverting the amplitude data. Fournier (2015) and Fournier et al. (2016a) then use that magnitude model only as a constraint in a full magnetization inversion with mixed-norm model objective function to achieve much more focused magnitude distribution with well-defined magnetization directions.

Synthetic and Field Examples

An example that highlights the capability of the mixed-norm inversion relates to inversion of the model in Figure 20, shown in a 3D perspective view and two sections. The model consists of two causative bodies with highly variable magnetization. The first is a simple block, and the second is a curved dyke with magnetization direction varying over a range of 90º. Figure 21 shows the corresponding total-field anomaly data simulated from this model. Figure 22 shows the inverted magnetization model (both magnitude and direction) through the cooperative magnetization inversion. Both the shape of the causative bodies and the magnetization direction in the inverted model are highly consistent with the true model in Figure 20. The magnetization direction is constrained implicitly by the requirement for the magnetization to reproduce the magnetic data and be confined in the compact regions with specific spatial orientations. If one considers the shape of the arcuate source to be formed by folding, this inversion is interesting in that it has recovered a case of pre-folding remanence.

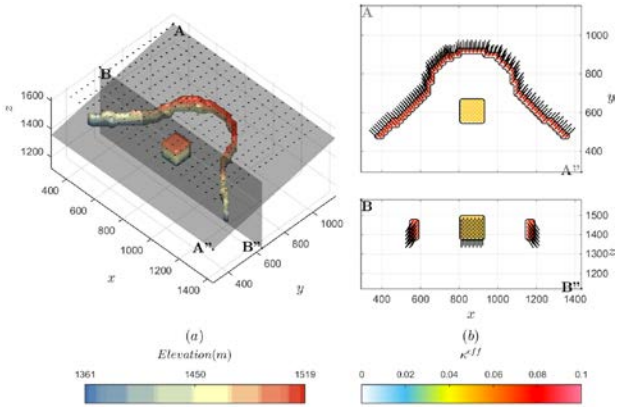

Figure 20: Perspective view and sections through the synthetic magnetization model. The arc-shaped anomaly is magnetized at an inclination of 45º and variable declinations between [-45º, 45º]. (Image form Fournier, 2015).

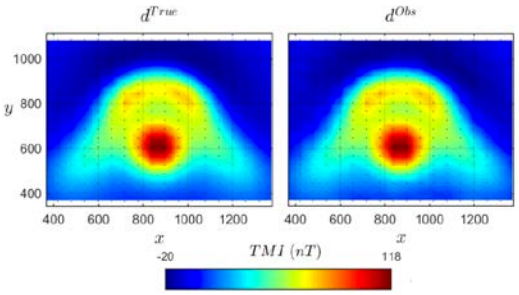

Figure 21: Data generated from the synthetic magnetization model. The two panels show respectively the accurate and noisy data. The latter is contaminated by random Gaussian noise with a 1 nT standard deviation. (Image form Fournier, 2015).

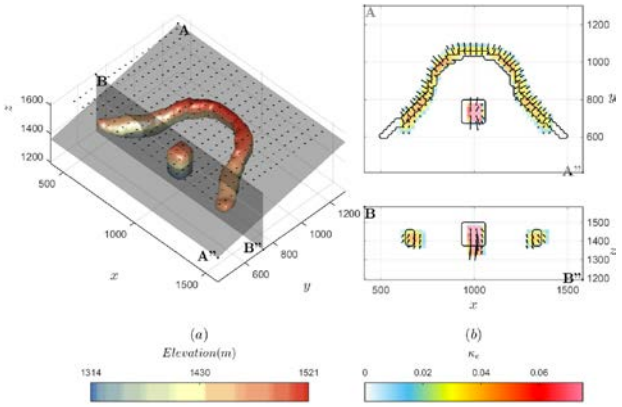

Figure 22: (a) Isosurface (0.01 SI) of effective susceptibility, and (b) sections A and B through the recovered magnetization model from the cooperative magnetization inversion algorithm. The depth extent of the causative bodies is indicated by both the color-coded elevation and the cross-section BB". Compact norms (p = 0; q = 2) were applied during the amplitude inversion. (Image form Fournier, 2015).

As a field example, the authors apply the algorithm to the well-known data set from Osborne copper-gold deposit, Australia. The data and a geologic cross-section are shown in Figure 23. This is a case with strong self-demagnetization so the magnetization direction is unknown and highly variable. Figure 24 shows the magnetization magnitude recovered from the amplitude data inversion using the mixed-norm objective function in the rotated coordinate systems and the corresponding magnetization model from the cooperative inversion using the mixed norms. Local coordinate systems aligned with the model features are obtained from the analyses of the magnetic data. The result is highly representative of the true source regions and associated magnetization directions. From the standpoint of matching the inverted magnetization magnitude with the known structure of the deposit, this inversion is one of the best results from magnetic inversion at this site.

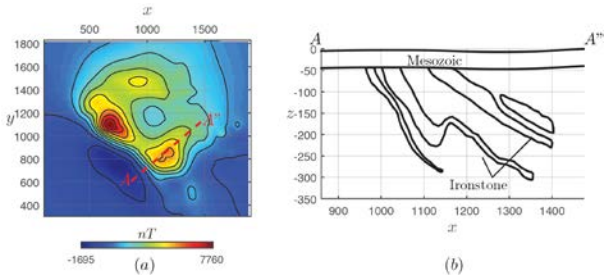

Figure 23: (a) Airborne magnetic data over the Osborne copper-gold deposit, Queensland. (b) Geological cross-section along A-A'. (Fournier et al, 2016a).

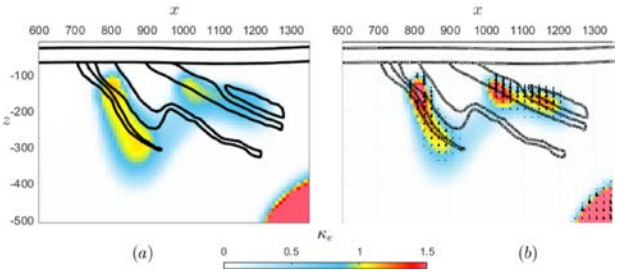

Figure 24: (a) Recovered effective susceptibility model from the amplitude inversion using a rotated sparse norm regularization, and (b) magnetization model from the cooperative magnetization inversion method. Each black dot with a line segment indicates a magnetization direction. (Fournier et al, 2016a).

Magnetization Inversion Using Fuzzy C-Means (FCM) Clustering

Li and Sun (2014, 2016) choose to impose a statistical constraint on the magnetization directions to explicitly restrict their variations, and develop an algorithm that seeks to recover a smooth magnetization model while allowing a small group of coherent magnetization directions.

Generalized inversion for magnetization allows each cell in the model to have its individual direction for maximum flexibility. The actual magnetization in geological units is often assumed to be rather uniform on the scales resolvable by magnetic data. If the magnetization of one geologic unit (or a large portion thereof) is uniform in direction, then directions should be constrained as a region-wise constant function during inversion. The inverted model should be characterized by a small number of magnetization directions, although these directions may be unknown prior to inversion.

This is precisely the type of constraint that the fuzzy c-means (FCM) clustering (e.g., Bezdek, 1981) can easily impose. Li and Sun (2014, 2016) use FCM to limit the magnetization directions to a small group of clusters in the same way that limits physical properties in a smooth inversion to a small number of values (e.g., Sun and Li, 2011; Lelièvre et al., 2012; Carter-McAuslan et al., 2015; Sun and Li, 2015). Li and Sun (2014, 2016) demonstrate the feasibility of FCM clustering for magnetization inversion and explore its potential for geology differentiation.

To work with the magnetization and its direction directly, Li and Sun (2016) employ the discretization scheme shown in equations 12 and 13, and additionally work with the unit vector of magnetization in each cell, $\hat{J}_j$.

The basic formulation of FCM-constrained magnetization inversion relies on the Tikhonov regularization and minimizes the total objective function in equation 15.

Given the assumption that the recovered magnetization should only align in a small number, c, of possible directions, Li and Sun (2016) add the following FCM term to the objective function in the Tikhonov regularization inversion,

$$\phi_{fcm} = \sum_{j=1}^{M}\sum_{k=1}^{C} u_{jk}^2 \left\| \hat{J}_j - \hat{v}_k \right\|^2 + \eta \sum_{k=1}^{c} \left\| \hat{v}_k - \hat{t}_k \right\|^2, \qquad (21)$$

where $\hat{J}_j$ is the unit vector in the magnetization direction in the jth model cell, $\hat{v}_k$ is the magnetization direction for the kth cluster found by the inversion, $\hat{t}_k$ is the kth dominant magnetization direction supplied as prior information, and u_{jk} is the probability that $\hat{J}_j$ belongs to the *k*th cluster. The membership function and cluster centers are the unknowns determined through the minimization of equation 21. The key to this algorithm is the choice of parameter c, which can be chosen based on priori information or through analyses by varying it in the inversion (Li and Sun, 2016).

In the absence of prior direction information, we may set $\eta = 0$ in equation 21. In that case the FCM objective function ϕ_{fcm} simply seeks to cluster the direction into *c* groups and find the cluster centers $\hat{v}_k$ in the inversion process. This is the generic FCM inversion. When prior information about the directions is available, $\eta > 0$ and the second term in equation 21 favours clusters close to the $\hat{t}_k$ directions. This approach is referred as the guided FCM clustering by Sun and Li (2015).

The objective function ultimately minimized is,

$$\phi(\vec{m}) = \phi_d(\vec{m}) + \beta\phi_m(\vec{m}) + \gamma\phi_{fcm}, \qquad (22)$$

where the parameter γ determines the relative importance of the FCM component. The regularization parameter β is chosen based on the desired data misfit, and the parameters γ and η are either prescribed a priori or determined during the inversion. The choice of these parameters remains an area of active research.

By combining the objective functions from (15) and (21), an inverted magnetization is sought with minimum structure spatially, and a small number of directions, and reproducing the magnetic data to within the error tolerance.

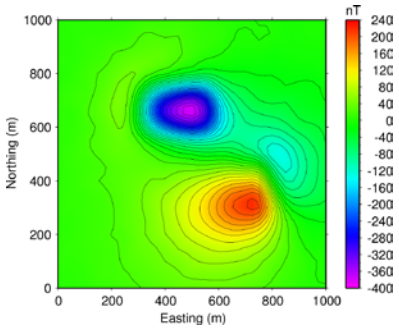

Figure 25: A set of synthetic total-field anomaly data produced by two causative bodies with different total magnetization. The inducing field has direction (I, D)=(65º,-25º).

Synthetic and Field Examples

Figure 25 shows a synthetic total-field data set produced by two source bodies whose magnetizations have similar magnitude but distinctly different directions. The rotation of the negative region away from declination in the southern anomaly and the dominantly negative northern anomaly indicate that magnetization directions of both source bodies are significantly different from the inducing field direction.

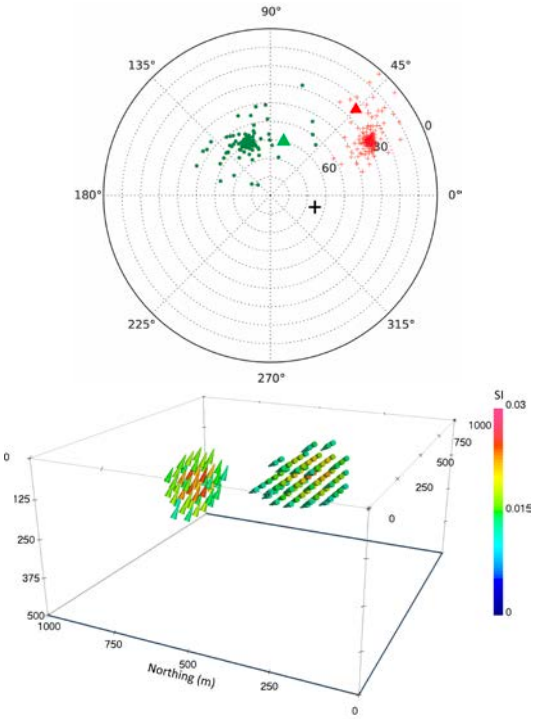

Figure 26: Magnetization directions recovered using the generic FCM clustering assuming two clusters. Top: The azimuth in the polar plot shows the declination of the magnetization direction and the radial axis shows the inclination with 90º in the center. Positive inclinations are plotted as red and negative as green. The inducing field direction is shown as the black +, the true magnetization directions of the two bodies are shown respectively as green and red triangles. Bottom: Corresponding 3D magnetization model with a cutoff value of 0.01 SI for the effective susceptibility.

Generic FCM clustering inversion was applied, assuming two magnetization directions (c=2). The recovered magnetization clusters corresponding to the two anomalies are displayed in a polar plot in Figure 26. The 3D magnetizations are also displayed in a perspective view as cones colored according to the effective susceptibility. Only cells with effective susceptibility above 0.01 SI are shown. The inverted magnetization is spatially coherent within the each causative body.

The markedly different magnetization directions suggest that the two sources could be geologically distinct. Although the difference in the magnetization can be inferred from visual inspection of the magnetic data, the quantification of the directions through inversion could provide more useful information. In practical application, such a result coupled with the magnetization magnitude could provide enough information to differentiate between different geological units. That is, they might have different geological origins or have gone through different structural movements relative to each other.

As a field example, Li and Sun (2016) invert the field data shown in Figure 4 to account for all anomalies. Figures 27 and 28 show the inversion result when three clusters are assumed, to account for the clearly reversely magnetized central anomaly, and the surrounding positive anomalies that may have remanent or purely induced magnetization.

The inverted magnetization directions displayed in Figure 27 show a cluster with an approximately -90º inclination corresponding to the central anomaly, a cluster with 36º inclination, and a third aligned with the nearly vertical inducing field. Examining the vector plot of the inverted magnetizations (Figure 28) reveals group-wise spatial coherency within the model domain such that magnetization direction is consistent within contiguous groups of model cells.

Both the synthetic and field data examples highlight an important strength of such a statistically constrained magnetization inversion, namely that multiple clusters can be specified without necessarily identifying the locations within the model to which each direction is applied.

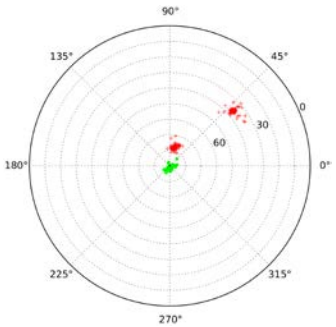

Figure 27: Polar plot of magnetization direction obtained from inverting the field data in Figure 4 by using a generic FCM algorithm with c=3. The inversion recovers one cluster with negative inclination (green dots) and two clusters with positive inclinations (red dots).

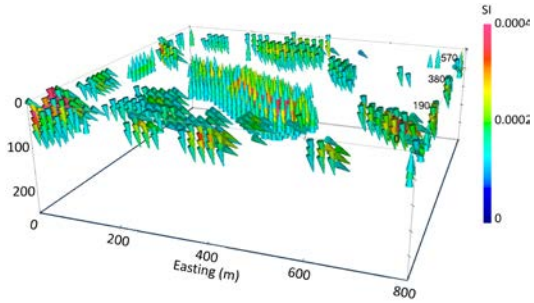

Figure 28: Vector plot of the recovered magnetization corresponding to that shown in Figure 27. The central cluster has a nearly -90º inclination and corresponds to the central negative anomaly in the data (Figure 4).

GEOLOGY DIFFERENTIATION USNG MAGNETIZATION DIRECTIONS

It has long been recognized that magnetization contains more information than can be extracted from its magnitude alone. The direction information has been used widely in the solid earth geophysics (e.g., Francheteau et al., 1970; Cordell and Taylor, 1971; Sager and Keating, 1984; Hildebrand and Staudigel, 1986). The magnitude of magnetization helps define the spatial shape and extent of the causative bodies and serves as indicator of volume fraction of magnetic minerals and, hence, lithology, while the magnetization directions could distinguish between different causative bodies with origins or having undergone different geological processes. Consequently, 3D magnetization inversion represents an attempt to fully utilize the information contained in magnetic data in the presence of remanent magnetization and, thereby, to assist in geology differentiation-based interpretation.

Deriving geological insights from analysis of magnetization is not a new idea, but now the field is at the stage where this objective approach can be pursued with the plethora of magnetization inversion algorithms. For instance, Lelièvre and Oldenburg (2009a) observe in a field data case that one part of the recovered model has significant magnetization perpendicular to the inducing field whereas the rest has little. It is clear that the two parts would be geologically different even if the magnitudes of magnetization are indistinguishable between the two.

To further illustrate this potential, we present an example of geology differentiation from Li and Sun (2016) for the data set shown in Figure 4. As the results in Figure 27 and 28 indicate, distinct magnetization directions are recovered when assuming three clusters. Thus, the model cells belonging to each cluster or dominant direction can be assigned as one distinct category of geological units. This is shown in Figure 29. Furthermore, the authors also attempt to calculate a confidence measure for the differentiation result from the consistency of recovered magnetization direction among inversions using different assumed numbers of clusters instead of attempting to determine an optimal number. Such differentiation of subsurface magnetic sources can then be interpreted more geologically instead of just magnetically.

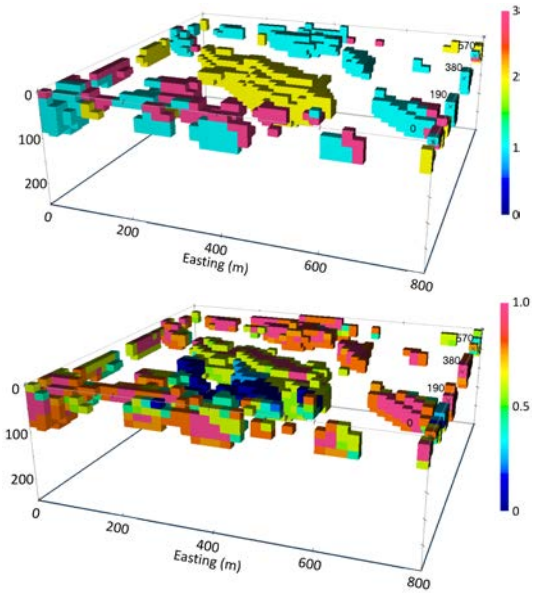

Figure 29: Top: Geology differentiation result based on the magnetization inversion of data in Figure 4 assuming three dominant directions. Category-0 corresponding to the background is not displayed. Bottom: confidence measure (1.0 being the highest) estimated from the variability of magnetization inversions assuming different numbers of possible directions.

Such efforts by various researchers are but a small step towards this exciting and potentially fruitful direction. The available examples in literature are limited at this point, but there is significant potential for deriving new information that are not available from visual inspection of data or interpretation based purely on magnetization magnitude. By using both magnitude and direction of magnetization, we may be able to address questions such as: (1) Do two different causative bodies have different origin or time of emplacement?; (2) Are their current magnetization directions consistent with the geological movement that produced the current structure?; or (3) Can we infer such structural movement using recovered magnetization directions and methodologies employed in paleomagnetic studies? We anticipate that such effort may be one of the major directions in the use of magnetization inversion in the coming decade.

CONCLUSIONS AND DISCUSSIONS

Generalized inversions for susceptibility developed in the 1990s brought about a paradigm change in the quantitative interpretation of magnetic data in exploration problems in the decade prior to Exploration ‘07. With the increased use of inversions, the challenges posed by the presence of remanent magnetization also came to the forefront. Consequently, much effort has been expended on this aspect of magnetic inversion in the last decade, and a plethora of approaches has been developed.

Several sophisticated parametric inversions using mixed-parametrizations with geometrically simple objects have been

developed that essentially pre-empty the challenges associated with the ambiguity introduced by the magnetization direction. These algorithms are now capable of handling complicated magnetic anomalies in practice.

The mixed susceptibility-magnetization inversion using the flexible vertical prism discretization of the model and incorporating specific geological boundaries represents a unique category that sequentially inverts for the susceptibility, remanent magnetization, and explicit geological boundary.

Generalized inversions that recover magnetization as a function spatial position, on the other hand, contend with the ambiguity in order to maintain the flexibility of the algorithms and develop different strategies to tackle the difficulty associated with the unknown magnetization direction. Within this, three categories of methods have been developed: (1) using estimated magnetization direction in susceptibility inversion, (2) inversion of direction-insensitive data such as magnetic anomaly amplitude and normalized source strength, and (3) magnetization inversion with different constraints. The majority of advances have occurred in the Category-3, which seeks to invert for magnetization as a vector function in 2D or 3D. We have discussed six approaches. The commonality is that they all impose some type of constraints on the variability of the recovered magnetization direction, either explicitly or implicitly.

Any magnetic data acquired in mineral exploration can now be inverted to construct a subsurface distribution of magnetization, either its magnitude or both magnitude and direction. Thereby, all magnetic data can be interpreted in a quantitative manner. It is now high time to utilize these advances made in the last decade. It is also important to understand the limitations and practical applicability of these methods.

Each method relies on one or more constraints based on general, conceptual, or site-specific prior information. For example, the parametric inversions relies on interactive modelling with multiple objects and works well with detailed investigation of specific magnetic anomalies; the mixed susceptibility-magnetization inversion requires site specific parameterization based on prior knowledge of geological structure information to fully utilize its potential. In terms of magnetization inversion, the approach of estimating the magnetization direction first is applicable to isolated compact anomalies; inversions of direction-insensitive amplitude data and NSS are inherently approximate in 3D and also require the conversion of total-field anomaly data to different forms; whereas the full magnetization inversion algorithms all require some constraint on the variability of magnetization directions or the relative magnitudes of induced and remanent magnetization.

The variety of available methods may appear daunting, and it indeed reflects the challenges faced with the inversion of magnetic data in the presence of strong remanent magnetization. However, the variety also shows a collective strength and presents the opportunity to tackle this important issue and extract useful information for exploration.

We have much to look forward to in the next decade. One interesting and potentially game-changing opportunity lies with the fact that, in addition to the information provided by the magnetization magnitude, the extra information embedded in the magnetization direction could be used to characterize source properties such as lithology through concentrations of magnetic minerals as well as to differentiate between different geological units. This possibility may foreshadow the next stage of development in magnetic interpretation.

ACKNOWLEDGEMENTS

I would like to thank P. Fullagar, D. Oldenburg, and J. McGaughey for their invitation to write this review. I would also like to thank D. Fournier, P. Fullagar, P. Lelièvre, D. Oldenburg, G. Pears, M. Pilkington, and M. Zhdanov for kindly providing some of the figures and/or data for generating figures used in this review paper. I am grateful for P. Fullargar's significant editorial effort. I would like to thank all my students and colleagues with whom I have had the pleasure to work on or discuss the quantitative interpretation of magnetic data affected by remanence and self-demagnetization.

REFERENCES

Bezdek, J. C., 1981, Pattern recognition with fuzzy objective function algorithms: Plenum Press.

Beiki, M., D. A. Clark, J. R. Austin, and C. Foss, 2012, Estimating source location using normalized magnetic source strength calculated from magnetic gradient tensor data: Geophysics, 77, J23–J37.

Bhattacharyya, B. K., 1966, A method for computing the total magnetization vector and the dimensions of a rectangular block-shaped body from magnetic anomalies: Geophysics, 31, 74-96.

Blakely, R., 1996, Potential theory in gravity and magnetic applications: Cambridge University Press.

Carter-McAuslan, A., P. G. Lelièvre, and C. G. Farquharson, 2015, A study of fuzzy c-means coupling for joint inversion, using seismic tomography and gravity data test scenarios: Geophysics, 80W1–W15

Clark, D. A., 2014, New approaches to dealing with remanence: magnetic moment analysis using tensor invariants and remote determination of in situ magnetisation using a static tensor gradiometer, ASEG Extended Abstracts 2013.

Clark, D.A., 2014, Methods for determining remanent and total magnetisations of magnetic sources – a review: Exploration Geophysics, 45(4), 271-304.

Coleman, C. and Y. Li, 2012, Quantitative Estimation of Error Level in Amplitude Inversion: 82nd Annual International Meeting, SEG, Expanded Abstracts, 5 p.

Coleman, C., 2014, Refining magnetic amplitude methodology for use in the presence of remanent magnetization: MSc. thesis, Colorado School of Mines.

Cordell, L., and P.T. Taylor, 1971, Investigation of magnetization and density of a north Atlantic seamount using Poisson's theorem: Geophysics, 36(5), 919-937.

Dampney, C.N.G., 1969, The equivalent source technique: Geophysics, 34, 39-53.

Dannemiller, N., and Y. Li, 2006, A new method for estimation of magnetization direction: Geophysics, 71, L69–L73.

Davis, K., and Y. Li, 2013, Efficient 3D inversion of magnetic data via octree-mesh discretization, space-filling curves, and wavelets: Geophysics, 78, J61-J73.

Davis, K., E. Haber, and D. Oldenburg, 2013, Large-scale magnetic inversion using differential equations and ocTrees: ASEG Extended Abstracts 2013.

Dransfield, M., A. Christensen, and G. Liu, 2003, Airborne vector magnetics mapping of remanently magnetized banded iron formations at Rocklea, Western Australia: Exploration Geophysics, 34, 93–96.

Ekblom, H., 1973, Calculation of linear best lp-approximation: BIT, 13, 292–300.

Ellis, R.G., B. de Wet, and I.N. Macleod, 2012, Inversion of magnetic data for remanent and induced sources: ASEG Extended Abstracts 2012.

Fedi, M., G. Florio, and A. Rapolla, 1994, A method to estimate the total magnetization direction from a distortion analysis of magnetic anomalies: Geophysical Prospecting, 42, 261–274.

Foss, C., and K. B. McKenzie, 2009, Strategies to model a suite of remanent magnetization anomalies: ASEG Extended Abstracts 2009, 1-18.

Foss, C., and B. McKenzie, 2011, Inversion of anomalies due to remanent magnetisation: An example from the Black Hill Norite of South Australia: Australian Journal of Earth Sciences, 58, 391–405.

Fournier, D., 2015, A Coperative Magnetic Inversion Method with Lp-norm Regularization: MSc Thesis, University of British Columbia.

Fournier, D., K. Davis, and D. Oldenburg, 2016a, Cooperative magnetic inversion: 86th Annual International Meeting, SEG, Expanded Abstracts, 1531-1536.

Fournier, D., D. Oldenburg, and K. Davis, 2016b, Robust and flexible mixed-norm inversion: 86th Annual International Meeting, SEG, Expanded Abstracts, 1542-1547.

Francheteau, J., C. Harrison, J. Sclater, and M. Richards, 1970, Magnetization of pacific seamounts: A preliminary polar curve for the northeastern Pacific: Journal of Geophysical Research, 75, 2035–2061.

Fullagar, P.K., and G.A. Pears, 2007, Towards geologically realistic inversion, in B. Milkereit ed., Proceedings of Exploration 07, 444-460.

Fullagar, P.K., G.A. Pears, and B. McMonnies, 2008, Constrained inversion of geological surfaces - pushing the boundaries: The Leading Edge, 27, 98-105.

Fullagar, P.K., and G.A. Pears, 2013, 3D magnetic modelling and inversion incorporating self-demagnetisation and interactions: ASEG Extended Abstracts 2013.

Fullagar, P.K., and G.A. Pears, 2015, Remanent magnetisation inversion: ASEG Extended Abstracts 2015.

Gerovska, D., M. J. Araúzo-Bravo, and P. Stavrev, 2009, Estimating the magnetization direction of sources from southeast Bulgaria through correlation between reduced-to-the-pole and total magnitude anomalies: Geophysical Prospecting, 57, 491–505.

Haney, M., and Y. Li, 2002, Total magnetization direction and dip from multiscale edges: 72nd Annual International Meeting, SEG, Expanded Abstracts, 735–738.

Haney, M., C. Johnston,Y. Li, and M. Nabighian, 2003, Envelopes of 2D and 3D magnetic data and their relationship to the analytic signal: Preliminary results: 73rd Annual International Meeting, SEG, Expanded Abstracts, 596–599.

Hansen, R. O., and R. S. Pawlowski, 1989, Reduction to the pole at low latitude by Wiener filtering: Geophysics, 54, 1607–1613.

Helbig, K., 1963, Some integrals of magnetic anomalies and their relationship to the parameters of the disturbing body: Zeitschrift für Geophysik, 29, 83–97.

Hildebrand, J., and H. Staudigel, 1986, Seamount magnetic polarity and cretaceous volcanism of the Pacific basin: Geology, 14, 456–458

Hou, C., 1979, Using potential field transformation to build an interpretation system of gravity and magnetic anomalies (in Chinese): Geophysical and Geochemical Exploration, 2, 21–10.

Kubota, R., and A. Uchiyama, 2005, Three-dimensional magnetization vector inversion of a seamount: Earth Planets Space, 57, 691–699.

Leão-Santos, M., Y. Li, and R. Moraes, 2015, Application of 3D magnetic amplitude inversion to iron oxide-copper-gold deposits at low magnetic latitudes: A case study from Carajás Mineral Province, Brazil: Geophysics, 80, B13-B22.

Lelièvre, P. G, 2009, integrating geologic and geophysical data through advanced constrained inversion: PhD thesis, University of British Columbia.

Lelièvre, P. G., and D.W. Oldenburg, 2009a, A 3D total magnetization inversion applicable when significant, complicated remanence is present: Geophysics, 74, 3, L21–L30.

Lelièvre, P.G. and D.W. Oldenburg, 2009b, A comprehensive study of including structural orientation information in geophysical inversions: Geophysical Journal International, 178, 623-637.

Li,Y., and D.W. Oldenburg, 1996, 3D inversion of magnetic data: Geophysics, 61, 394–408.

Li, Y., and D.W. Oldenburg, 2000a, Joint inversion of surface and three-component borehole magnetic data: Geophysics, 65, 540-552.

Li, Y. and D.W. Oldenburg, 2000b, Incorporating geological dip information into geophysical inversions: Geophysics, 65, 148-157.

Li,Y., and D.W. Oldenburg, 2003, Fast inversion of large-scale magnetic data using wavelet transforms and a logarithmic barrier method: Geophysical Journal International, 152, 251–265.

Li, Y., and D. Oldenburg, 2010, Rapid construction of equivalent sources using wavelets: Geophysics, 75, L51-L59

Li, Y., S. Shearer, M. Haney, and N. Dannemiller, 2010, Comprehensive approaches to the inversion of magnetic data affected by remanent magnetization: Geophysics, 75. L1–L11.

Li, Y., Z. He, and Y. Liu, 2012, Application of magnetic amplitude inversion in exploration for volcanic units in a basin environment: Geophysics, 77, B219-B225.

Li, S.L. and Y. Li, 2014, Inversion of magnetic anomaly on rugged observation surface in the presence of strong remanent magnetization: Geophysics, 79, J11-J19.

Li, Y. and J. Sun, 2014, Total magnetization vector inversion using guided fuzzy c-means clustering: 84th Annual International Meeting, SEG, Expanded Abstracts, 1285-1290.

Li, Y. and J. Sun, 2016, 3D magnetization inversion using fuzzy c-means clustering with application to geology differentiation: Geophysics, 81, J61-J78.

Liu, S., X. Hu, T. Liu, J. Feng, W. Gao, and L. Qiu, 2013, Magnetization vector imaging for borehole magnetic data based on magnitude magnetic anomaly: Geophysics, 78, D429–D444

Liu, S., X. Hu, Y. Xi, T. Liu, and S. Xu, 2015, 2D sequential inversion of total magnitude and total magnetic anomaly data affected by remanent magnetization: Geophysics, 80, K1-K12.

Lourenco, J. S., and H.F. Morrison, 1973, Vector magnetic anomalies derived from measurements of a single component of the field: Geophysics, 38, 359–368.

MacLeod, I.N. and R. G. Ellis, 2013, Magnetic Vector Inversion, a simple approach to the challenge of varying direction of rock magnetization: ASEG Expanded Abstracts 2013.

Medeiros, W.E., and J.B.C. Silva, 1995, Simultaneous estimation of total magnetization direction and 3D spatial orientation: Geophysics, 60, 1365-1377.

Mendonça, C. A., 2004, Automatic determination of the magnetization–density ratio and magnetization inclination from the joint interpretation of 2D gravity and magnetic anomalies: Geophysics, 69, 938-948.

Morris, B., H. Ugalde, and V. Thomson, 2007, Magnetic remanence constraints on magnetic inversion models: The Leading Edge, 26, 960-964.

Mueller, E. L., W. A. Morris, P.G. Killeen, and S. Balch, 1997, Combined 3-D interpretation of airborne, surface, and borehole vector magnetics at the McConnell nickel deposit, in A.G. Gubins, ed., Proceedings of Exploration 97, 657-666.

Nabighian, M., 1972, The analytic signal of two-dimensional magnetic bodies with polygonal cross-section: Its properties and use for automated anomaly interpretation: Geophysics, 37, 507–517.

Nabighian, M., 1984, Towards a three-dimensional automatic interpretation of potential field data via generalized Hilbert transforms: Fundamental relations: Geophysics, 49, 780-786

Paine, J., M. Haederle, and M. Flis, 2001, Using transformed TMI data to invert for remanently magnetised bodies: Exploration Geophysics, 32, 238–242.

Pedersen, L. B., 1978, Wavenumber domain expressions for potential fields from arbitrary 2-, 21/2-, and 3-dimensional bodies: Geophysics, 43, 626–630.

Pedersen, L. B., and M. Bastani, 2016, Estimating rock-vector magnetization from coincident measurements of magnetic field and gravity gradient tensor: Geophysics, 81, B55-B64.

Phillips, J. D., 2005, Can we estimate total magnetization directions from aeromagnetic data using Helbig's formulas: Earth, Planets, and Space, 57, 681–689.

Pilkington, M., 1997, 3-D magnetic imaging using conjugate gradients: Geophysics, 62, 1132–1142.

Pilkington, M. and M. Beiki, 2013, Mitigating remanent magnetization effects in magnetic data using the normalized source strength: Geophysics, 78, J25-J32.

Portniaguine, O, and M.S. Zhdanov, 2002, 3-D magnetic inversion with data compression and image focusing: Geophysics, 67, 1532-1541.

Pratt, D.A., K.B. McKenzie, and A.S. White, 2012. The remote determination of magnetic remanence: ASEG Extended Abstracts 2012.

Roest, W. R., J. Verhoef, and M. Pilkington, 1992, Magnetic interpretation using the 3-D analytic signal: Geophysics, 57, 116-125.

Roest, W., and M. Pilkington, 1993, Identifying remanent magnetization effects in magnetic data: Geophysics, 58, 653–659.

Sager, W., and B. Keating, 1984, Paleomagnetism of Line Islands seamounts: Evidence for late cretaceous and early tertiary volcanism: Journal of Geophysical Research: Solid Earth, 89, 11135–11151

Schmidt, P.W., and D.A. Clark, 1998, The calculation of magnetic components and moments from TMI: A case study from the Tuckers igneous complex, Queensland: Exploration Geophysics, 29, 609–614.

Schmidt, P., D. Clark, K. Leslie, M. Bick, D. Tilbrook, and C. Foley, 2004, GETMAG a SQUID magnetic tensor gradiometer for mineral and oil exploration: Exploration Geophysics, 35, 297–305.

Shearer, S., 2005, Three-dimensional inversion of magnetic data in the presence of remanent magnetization: M.Sc. thesis, Colorado School of Mines.

Shearer, S., and Y. Li., 2004, 3D Inversion of magnetic total-gradient data in the presence of remanent magnetization: 74th Annual International Meeting, SEG, Expanded Abstracts, 774–777.

Shi, Z., M. den Hartog, L. Pryer, Y.P. Djomani, and K. Connors, 2013, A new technique for low magnetic latitude transformation: Synthetic model results and examples.: ASEG Extended Abstracts 2013.

Silva, J. B. C., and G.W. Hohmann, 1981, Interpretation of three component borehole magnetometer data: Geophysics, 46, 1721–1731.

Stavrev, P. and D. Gerovska, 2000, Magnetic field transforms with low sensitivity to the direction of source magnetization and high centricity: Geophysical Prospecting, 48, 317-340.

Sun, J., and Y. Li, 2011, Geophysical inversion using petrophysical constraints with application to lithology differentiation: 81st Annual International Meeting, SEG, Expanded Abstracts, 2644–2648.

Sun, J., and Y. Li, 2014, Adaptive Lp inversion for simultaneous recovery of both blocky and smooth feature in geophysical model: Geophysical Journal International, 197, 882–899.

Sun, J., and Y. Li, 2015, Multidomain petrophysically constrained inversion and geology differentiation using guided fuzzy c-means clustering: Geophysics, 80 (4), ID1–ID18.

Wang, M. Q., Q. Di, K. Xu, and R. Wang, 2004, Magnetization vector inversion equations and forword [sic] and inverse [sic] 2-D model study (in Chinese): Chinese Journal of Geophysics, 47, 601–609.

Watts, A., 1997, Exploring for nickel in the 90s, or 'til depth us do part', in A.G. Gubins ed., Proceedings of Exploration 97, 1003-1014.

Wilson, H. S., 1985, Analysis of the magnetic gradient tensor: Defence Research Establishment Pacific, Technical Memorandum 8, 5–13.

Zhu, Y., M.S. Zhdanov, and M. Čuma, 2015, Inversion of TMI data for the magnetization vector using Gramian constraints: 85th Annual International Meeting, SEG, Expanded Abstracts, 1602-1606.